Journal of Electrochemistry

Volume 28
Issue 3 *Special Issue: Frontier of Electrochemistry (Ⅱ)*

2022-03-28

In-Situ/ Operando^{57}Fe Mössbauer Spectroscopic Technique and Its Applications in NiFe-based Electrocatalysts for Oxygen Evolution Reaction

Jafar Hussain Shah

Qi-Xian Xie

Zhi-Chong Kuang

Ri-Le Ge

Wen-Hui Zhou

Duo-Rong Liu

Alexandre I. Rykov

See next page for additional authors

Recommended Citation

Jafar Hussain Shah, Qi-Xian Xie, Zhi-Chong Kuang, Ri-Le Ge, Wen-Hui Zhou, Duo-Rong Liu, Alexandre I. Rykov, Xu-Ning Li, Jing-Shan Luo, Jun-Hu Wang. *In-Situ/ Operando*^{57}Fe Mössbauer Spectroscopic Technique and Its Applications in NiFe-based Electrocatalysts for Oxygen Evolution Reaction[J]. *Journal of Electrochemistry*, 2022 , 28(3): 2108541.
DOI: 10.13208/j.electrochem.210854
Available at: https://jelectrochem.xmu.edu.cn/journal/vol28/iss3/3

In-Situ/Operando ^{57}Fe Mössbauer Spectroscopic Technique and Its Applications in NiFe-based Electrocatalysts for Oxygen Evolution Reaction

Authors

Jafar Hussain Shah, Qi-Xian Xie, Zhi-Chong Kuang, Ri-Le Ge, Wen-Hui Zhou, Duo-Rong Liu, Alexandre I. Rykov, Xu-Ning Li, Jing-Shan Luo, and Jun-Hu Wang

Corresponding Author(s)

Jun-Hu Wang(wangjh@dicp.ac.cn)

This protocol is available in Journal of Electrochemistry: https://jelectrochem.xmu.edu.cn/journal/vol28/iss3/3

电 化 学
J. Electrochem. 2022, 28(3), 2108541 (1 of 31)

[Protocol] DOI: 10.13208/j.electrochem.210854 Http://electrochem.xmu.edu.cn

In-Situ/Operando ^{57}Fe Mössbauer Spectroscopic Technique and Its Applications in NiFe-based Electrocatalysts for Oxygen Evolution Reaction

Jafar Hussain Shah[1], Qi-Xian Xie[2], Zhi-Chong Kuang[1], Ri-Le Ge[1], Wen-Hui Zhou[1], Duo-Rong Liu[1], Alexandre I. Rykov[1], Xu-Ning Li[1], Jing-Shan Luo[2], Jun-Hu Wang[1*]

(*1. Center for Advanced Mössbauer Spectroscopy, Mössbauer Effect Data Center, Dalian Institute of Chemical Physics, Chinese Academy of Sciences, Dalian 116023, Liaoning, China; 2. Institute of Photoelectronic Thin Film Devices and Technology, Key Laboratory of Photoelectronic Thin Film Devices and Technology of Tianjin, Ministry of Education Engineering Research Center of Thin Film Photoelectronic Technology, Renewable Energy Conversion and Storage Center, Nankai University, Tianjin 300350, China*)

Abstract: The development of highly efficient and cost-effective electrocatalysts for the sluggish oxygen evolution reaction (OER) remains a significant barrier to establish effective utilization of renewable energy storage systems and water splitting to produce clean fuel. The current status of the research in developing OER catalysts shows that NiFe-based oxygen evolution catalysts (OECs) have been proven as excellent and remarkable candidates for this purpose. But it is critically important to understand the factors that influence their activity and underlying mechanism for the development of state-of-the-art OER catalysts. Therefore, the development of *in-situ*/*operando* characterizations is urgently required to detect key intermediates along with active sites and phases responsible for OER. ^{57}Fe Mössbauer spectroscopy is one of the appropriate and suitable techniques for determining the phase structure of catalysts under their electrochemical working conditions, identifying the active sites, clarifying the catalytic mechanisms, and determining the relationship between catalytic activity and the coordination structure of catalysts. In this tutorial review, we have discussed the current status of research on NiFe-based catalysts with particular attention to introduce in detail the knowhow about the development and utilization of *in-situ*/*operando* ^{57}Fe Mössbauer-electrochemical spectroscopy for the study of OER mechanism. A brief overview using NiFe-(oxy)hydroxide catalysts, derived from ordered porous metal-organic framework (MOF) material NiFe-PBAs (Prussian blue analogues), as a typical model study case for the OER electrocatalyst and self-designed *in-situ*/*operando* ^{57}Fe Mössbauer-electrochemical instrument, has been provided for the better understanding of readers. Moreover, using *in-situ*/*operando* ^{57}Fe Mössbauer spectroscopy, the crucial role of Fe species during OER reaction has been explained very well.

Key words: oxygen evolution reaction; NiFe-(oxy)hydroxide electrocatalyst; NiFe Prussian blue analogue; *in-situ*/*operando* ^{57}Fe Mössbauer spectroscopy; key intermediate detection

1 Introduction

In recent decades, increasing demand for energy and severe environmental implications have spurred the switch from fossil fuels to cleaner energy (such as solar, wind, and tidal energies)[1]. However, owing to daily, seasonal, and regional variables, these renewable energies are unpredictable, restricting their significant success in the global energy mix. Water split-

Cite as: Shah J H, Xie Q X, Kuang Z C, Ge R L, Zhou W H, Liu D R, Rykov A I, Li X N, Luo J S, Wang J H. *In-situ*/*operando* ^{57}Fe Mössbauer spectroscopic technique and its applications in NiFe-based electrocatalysts for oxygen evolution reaction. *J. Electrochem.*, 2022, 28(3): 2108541.

Received: 2021-12-14, Revised: 2022-01-24. *Corresponding author, Tel: (86-411)84379159, E-mail: wangjh@dicp.ac.cn

ting devices, rechargeable metal-air batteries, polymer electrolyte membrane fuel cells (PEMFCs) and CO_2 reduction are several kinds of novel energy conversion and storage technologies[2-6]. Even though the architecture of these devices differs, the fundamental processes are almost the same. In a rechargeable metal-air battery, metal dissolution and deposition on the negative electrode (metal), while the oxygen reduction reaction (ORR) and oxygen evolution reaction (OER) on the positive electrode (air)[2]. For the electrochemical CO_2 reduction reaction (CO_2RR), the OER process can serve as the anode reaction[7]. An unmet challenge for this reaction is the lack of efficient oxygen evolution electrocatalysts (OECs), using a non-noble metal electrocatalyst to pair with the CO_2RR process for high overall energy conversion efficiency[7]. On the other hand, electrochemical water splitting, which is known as the most viable way of producing pure hydrogen quickly and an indirect way of storing electrical energy obtained from intermittent sources in the form of chemical fuels like H_2, comprises two half-cell reactions: hydrogen evolution reaction (HER) at the cathode and OER at the anode[8-9]. The overall reaction is predicted to occur at 1.23 V vs. RHE ($2H_2O \rightarrow 2H_{2(g)} + O_{2(g)}$ where E = 1.23 V)[10]. However, large overpotentials associated with both OER and HER prevent this. The general alkaline OER process in water splitting is summarized in Figure 1[11]. OER is the kinetically sluggish one because it involves four protons and four electrons coupled transfer with the formation of an oxygen-oxygen (O-O) bond in which each elementary step has its own activation energy. And the one with the highest activation energy is the slowest elementary step, making it the rate-determining step in OER[12]. Therefore, OER dominates the overall efficiency of the two technologies because it pertains to the creation of O-O bonds and includes four proton-coupled electron transfer processes[13-14]. As a result, highly OECs are required to accelerate the OER or decrease the overpotential to mitigate the energy loss inherent in energy conversion technologies.

The innovative combination of materials science and water splitting electrochemistry opens new pathways for creating different OECs. IrO_2 and RuO_2 are considered as benchmark catalysts due to their low onset potentials for triggering the OER. However, small reserves and high prices restrict their utilization at a larger scale[15-16]. To address these problems associated with rare earth elements, scientists have focused on non-precious metals-based OECs, mostly composed of 3d transition metals[17-18]. In the start, oxides and hydroxides of these 3d transition metals-based OECs have been investigated under alkaline conditions[15]. Beyond oxides and hydroxides, significant efforts have been dedicated to develop highly efficient electrocatalysts for OER from cost-effective and naturally abundant materials, such as layer structure materials[18], metal chalcogenides[19], metal nitrides[20], metal phosphide[21], metal borides[22],

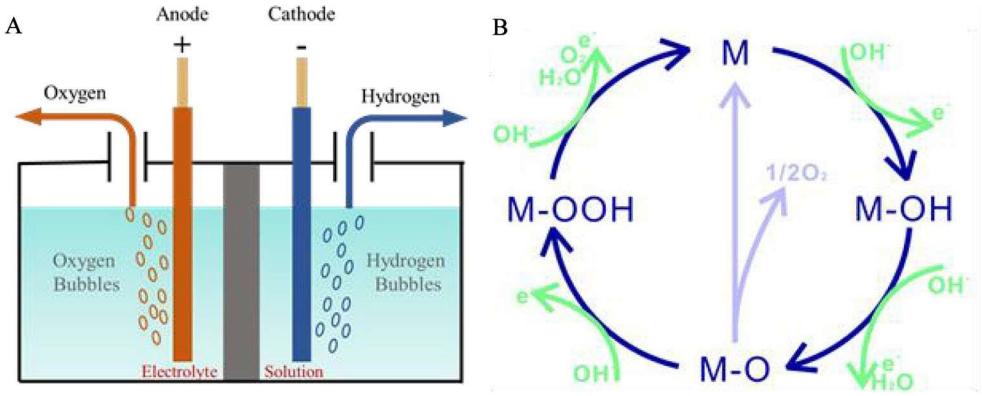

Figure 1 (A) Schematic of the electrochemical water splitting; (B) The reported OER mechanism for alkaline conditions[11]. Copyright@The Royal Society of Chemistry 2019. Reproduced with permission. (color on line)

metal carbides[23], and organometallics[24]. According to recent studies, all non-precious metal catalysts containing anions other than oxides and hydroxides undergo surface chemical reconstruction, resulting in the production of oxides/hydroxides on the surface in contact with the alkaline electrolyte[25,26]. As a result, regardless of the materials utilized for OER under alkaline circumstances, their (oxy)hydroxides are always the real-time catalyst during OER. Among these transition metal (oxy)hydroxides materials, NiFe-(oxy) hydroxides have been proved to be the most potential materials in alkaline electrolytes[27]. According to many studies, pure Ni and Fe oxides/hydroxides are not efficient OER electrocatalysts, while their complexes have shown higher OER activity[28].

2 Recent Progress and Understanding of Fe Role in Ni-Based Electrocatalyst

The most active electrocatalyst for OER was thought to be $Ni(OH)_2$/NiOOH at the start of the evolution of 3d transition metals-based OECs. Subbaraman and co-workers suggested that the OER activity trend of 3d transition metal divalent cations goes in the order of $Mn^{2+} < Fe^{2+} < Co^{2+} < Ni^{2+}$[29]. And it was believed to be true and accepted widely until it was found that a trace amount of Fe (~ 1 ppm) largely enhanced the OER activity of Ni^{2+} based electrocatalysts[30-31]. In the late 1980s, the extraordinary OER performance of $Ni(OH)_2$ anodes-based alkaline batteries was observed in Fe-containing (up to 1 ppm) KOH electrolyte with smaller cell voltages than pure KOH[32]. This work found that Fe doping from the electrolyte into the $Ni(OH)_2$ electrode reduced both the cell voltage and the OER onset overpotential in an alkaline medium. And this was the first time that researchers discovered the Fe effect on increasing the OER activity of $Ni(OH)_2$. It was observed that the OER activity of a Fe-doped β-$Ni(OH)_2$ electrocatalyst increases linearly as the quantity of Fe is high enough to enter the β-$Ni(OH)_2$ lattice. And as a result, it was assumed that Fe might be the active site for OER[33]. Therefore, Ni-based OECs attracted great attention, and a huge amount of research was conducted to determine the processes by which Fe improves the OER activity of Ni-based OECs.

Without a doubt, Fe incorporation has been the driving force behind the significant OER improvement seen with Ni-based OECs in unpurified, reagent grade KOH electrolyte so far. OER activities were being massively reported for these materials without realizing that Fe in concentration as low as 1 ppm may significantly change the OER activities of Ni-based OECs. Based on these findings, much research has been published in literatures detailing the various functions of Fe in the matrix of Ni-based OECs. Important roles stated in literatures with experimental pieces of evidence are: 1) Incorporation of Fe in place of Ni in their respective hydroxides/(oxy) hydroxides matrices makes them harder to be oxidized further and thus alters the redox electrochemistry of Ni, 2) When Fe is incorporated into Ni-based OECs, it causes structural changes, 3) It is well-known fact that Fe^{3+} serves as the strongest transition metals-based Lewis acid with a stronger electrophilic nature and notably affects the electronic properties of the other cations in which being incorporated; hence it changes the Ni oxidation states and aids in the formation of active Ni^{4+} sites, and 4) Fe^{3+} ions in NiFe-based OECs with a 1:0.33 ratio depicts a superexchange magnetic contact that improves OER electrocatalysis by allowing electrons to hop.

Almost all researches involving Ni-based OECs and Fe incorporation have revealed that the most appropriate and active composition of Ni:Fe for OER is 1:0.2 ~ 0.3. NiOOH is an excellent electronic conductor, with no change in conductivity before and after Fe inclusion. Boettcher and co-workers have recently discovered that the effective conductivity of NiOOH films diminishes as the cycle number increases and becomes independent of the quantity of Fe incorporated into the film[34]. The decrease in conductivity with increasing cycle number did not affect the OER activity and substantially increased. Figure 2 illustrates the cyclic voltammetric (CV) cycles of a NiOOH film electrode in a KOH electrolyte with and without Fe-spiking, demonstrating an increase in OER

activity despite a reduction in effective conductivity. As a result, it is apparent that the observed increase could not be attributed only to the change in conductivity that occurs when Fe is incorporated into Ni-based OECs. The fact that Fe in FeOOH is insulating, which is a big contradiction. In this way, how could it improve the conductivity of NiOOH when combined? Bell and co-workers proposed a plausible mechanism in which Fe^{3+} ions were incorporated into β-NiOOH lattices in smaller amounts and exhibited an extraordinarily shrunken Fe-O bond length, resulting in Fe^{3+} sites in NiOOH lattice getting the required conductivity not from their incorporation but from the conductivity of NiOOH lattice. They also discovered that increasing Fe concentration results in the development of insulating FeOOH surfaces, which decreases the OER activity. The incorporation of Fe into Ni-based OECs could increase the OER activities, which was ascribed to the change in effective conductivity (potential dependent), but it cannot be the sole one reason.

Fe incorporation or doping has a significant impact on electrochemical oxidation and reduction characteristics of $Ni(OH)_2$. The incorporation of Fe effect was first observed from the shifting of the $Ni(OH)_2$ oxidation peak to NiOOH during electrochemical water oxidation[35]. Boettcher and co-workers observed comparable anodic shifts of $Ni(OH)_2$ → NiOOH oxidation peak when aged the electrodeposited $Ni(OH)_2$ film in TraceSelect KOH (~ 36 ppb Fe) and reagent grade KOH (~ 1 ppm Fe) for 1 hour (Figure 3(A-E))[36]. When the Fe concentration reached 5%, they found a similar change in the Ni:Fe co-deposited film in pure KOH (Fe free). However, there was no such anodic shift in $Ni(OH)_2$ → NiOOH oxidation peak in the Ni:Fe co-deposited film with 25% Fe content. The most intriguing result of this research was the reduction in the strength of the $Ni(OH)_2$ → NiOOH oxidation peak when aged in Fe-free KOH and the development of a new peak at a high overpotential, which was ascribed to the production of Ni^{4+} ions. They also discovered that OER activity was reduced with aging time and attributed it to the reduction in structural flaws in $Ni(OH)_2$. However, $Ni(OH)_2$ films aged in TraceSelect KOH (~ 36 ppb Fe) and reagent grade KOH (~ 1 ppm Fe) showed a substantial increase in OER activity. This suggests that incorporation of Fe boosts activity, although the anodic shift of $Ni(OH)_2$ → NiOOH oxidation peak in these cases is opposite to what was anticipated. Furthermore, aging had no effect on the co-deposited NiFe-(oxy)hydroxide films. They concluded that the OER activity is intrinsic to NiFe-(oxy)hydroxide sheets and not linked to structural flaws in $Ni_{0.75}Fe_{0.25}OOH$. However, the observed anodic shift of $Ni(OH)_2$ → NiOOH oxidation peak in their research could not be fully explained.

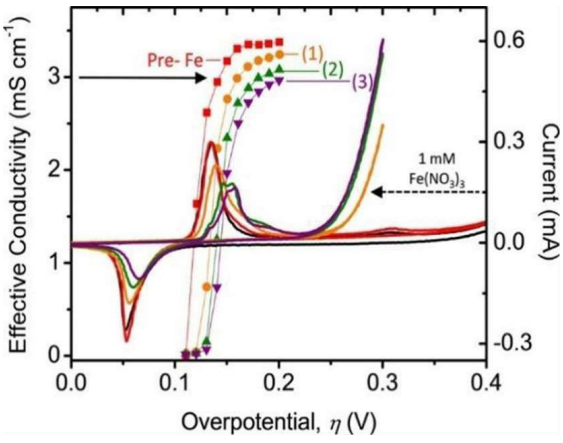

Figure 2 Steady-state effective conductivity of NiO_xH_y on an interdigitated array (IDA) electrode as a function of Fe incorporation from 1 mmol·L^{-1} $Fe(NO_3)_3$ in a 1 mol·L^{-1} aqueous KOH solution [34]. Copyright© 2017 American Chemical Society. Reproduced with permission. (color on line)

Later on, Strasser and co-workers published an intriguing result based on their *in-situ*/*operando* differential electrochemical mass spectrometric (DEMS) and X-ray absorption spectroscopic (XAS) studies on NiFe mixed oxides under OER conditions[37]. In this research, they discovered that nearly all Fe^{3+} ions in NiFe mixed oxides remained in the oxidation state of 3+, and that 75% of Ni remained in the 2+ and 3+ states, while the remaining Ni was oxidized to the 4+ state (shown in Figure 4(A-B)). These findings were remarkably similar to those previously reported[36]. Furthermore, they hypothesized that the kinetic competition between metal oxidation and metal reduction

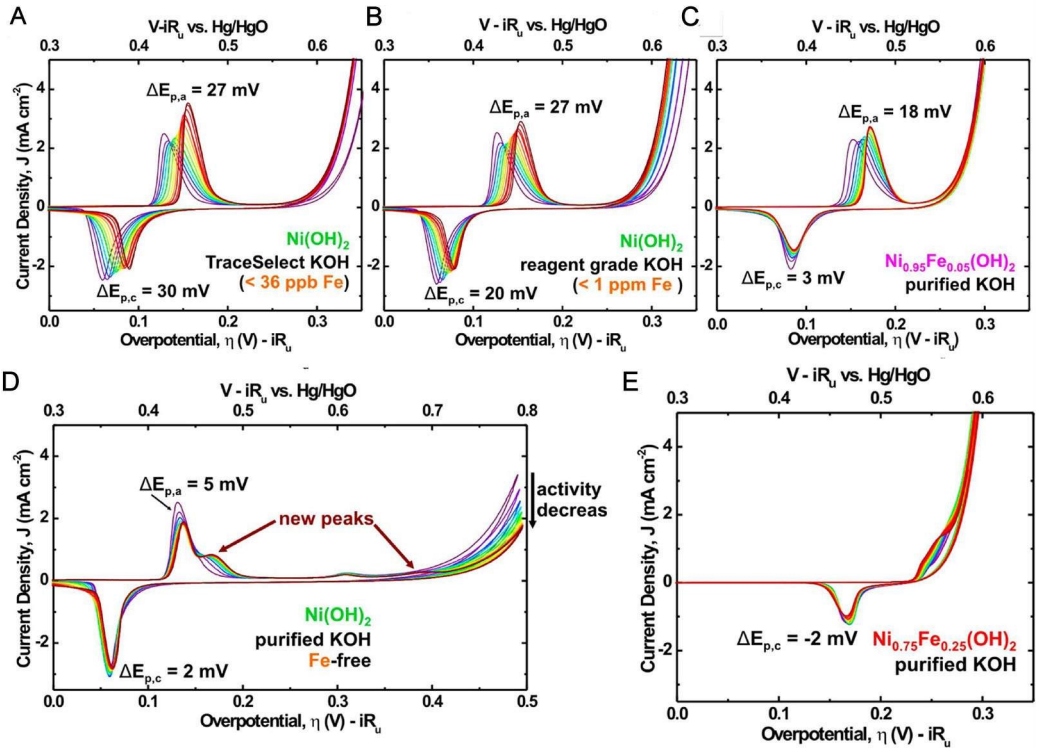

Figure 3 Cyclic voltammograms were taken during the aging of films in various purities of KOH. A total of 13 CV scans are shown for each sample: one for the initial as-deposited film (the dark purple), and one additional scan after each 5 min aging period up to a total of 1 hour of aging (the dark red). The changes in the anodic and cathodic peak positions ($\Delta E_{p,a}$ and $\Delta E_{p,c}$) are labeled for each set of CVs. ($\Delta E_{p,a}$ value is shown for the $Ni_{0.75}Fe_{0.25}(OH)_2$, as the oxidation peak is partially obscured by the OER current.)[36] Copyright©2014 American Chemical Society. Reproduced with permission. (color on line)

during O_2 evolution may be responsible for insignificant detectable high valence metal deposition[38]. When there was no Fe or very little Fe (less than 10%), the kinetic competition preferred metal oxidation, but when there was a lot of Fe, the kinetic rivalry favored the metal reduction phase during O_2 evolution. This means that for the substantial OER improvemnet in NiFe mixed oxide catalysts, the required concentration of Fe should be more than 10%. Moreover, in their explanation for why the oxidation peak strength of the $Ni(OH)_2 \rightarrow NiOOH$ decreased with increasing Fe content was also the kinetic competition and this resulted in most of the Ni remained unoxidized upon polarization in the 2+ state. This is the main reason that anodic shift for (oxy)hydroxide peak occurred in Ni-based OECs. The faradic efficiency of OER decreased with increasing the oxidation ($Ni(OH)_2 \rightarrow$ NiOOH) peak which rises as the pH of the reaction rises. The findings of this research highlight the importance of Fe concentration, electrolyte strength, and support material during catalyst fabrication. Although there is an explanation for why anodic shift and intensity drop occur in Ni-based OECs with increasing Fe content, but enhancing mechanism by redox inactive Fe^{3+} ions is still a subject of ambiguity.

Gray and colleagues recently published comparable findings in a study of NiFe-LDH (LDH: layered double hydroxide) inducing OER in water-depleted conditions, i.e., in acetonitrile[39]. They discovered the production of a cis-dioxo-Fe(IV) intermediate immediately before OER. They found that when this intermediate was separated and put into neutral water, it produced hydrogen peroxide, and generated oxygen in case of alkaline water. This was one of the strongest arguments indicating and supporting Fe^{4+} ions formation in the presence of Ni during catalyzing water oxidation, whereas previously it was claimed that some parts of Ni were changed to 4+ oxidation

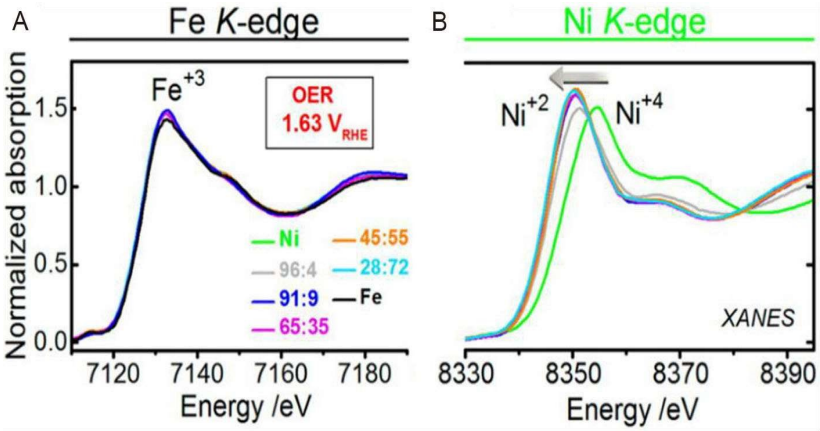

Figure 4 *In-situ/operando* XAS of the NiFe OER catalysts with varying catalyst composition $Ni_{100-x}Fe_x$: (A) Fe *K*-edges and (B) Ni *K*-edges[37]. Copyright©2016 American Chemical Society. Reproduced with permission. (color on line)

state upon Fe incorporation. It was also discovered that the highly active $Ni_xFe_{1-x}OOH$ catalyst has two active sites with remarkable difference in OER rate constants, and the percentage of fast sites matched well with the fraction of Fe in the catalyst[40]. These findings clarified that Fe and Ni, both are active sites for OER, with Fe sites being significantly faster. This may be due to the optimal bond energies of intermediates when coordinated with Fe. On the other hand, OER intermediates have a weaker adsorption contact with Ni where they create more covalent M-O bonds, which need a larger potential to break in order to develop O_2. This is why, in the absence of Fe, $Ni(OH)_2$ needs a greater overpotential to start the oxygen evolution.

As a result of these massive efforts to understand the intrinsic phenomena, phase, and structure of NiFe-based OECs, researchers have reported several conflicting findings. Here are some common and general findings from past researches: 1) Fe^{3+} incorporation/doping into NiOOH generates a greater number of catalytically active sites than a simple rock salt structure with hydroxides, and the content of Fe^{3+} dissolves up to 25% into $Ni(OH)_2$/NiOOH matrices under applied voltages or during electrolyte aging, making it a superior OEC[41]. 2) The production of Ni^{4+} is reduced when Fe^{3+} concentration rises[37]. 3) The active site is Fe^{3+}, although it is inactive when presented alone as FeOOH at lower overpotentials. This is because the only first monolayer of FeOOH is OER active and electrolyte-permeable at lower overpotentials[42]. 4) The active sites are Fe^{3+} ions that replaced Ni^{3+} ions in NiOOH matrices at the edges, corners, and defect sites. Those who are deeply embedded in the majority of NiOOH do not take part in OER[34]. 5) The active Ni^{2+} ions are simply stabilized by Fe^{3+}, as indicated by the anodic shift of the $Ni(OH)_2 \rightarrow$ NiOOH oxidation peak with the decreased integrated charge[38]. 6) Fe^{3+} ions have a 6-percent shorter Fe-O bond length in NiOOH matrices, suggesting that Fe^{3+} ions may have partly higher oxidation states, and active sites in both NiFe systems are anticipated to be Fe^{3+}. The conductive medium needed for Fe^{3+} to catalyze OER is provided by NiOOH matrices[43]. 7) Fe^{3+} in the conductive Fe_7S_8 phase is OER active in the same way as Fe^{3+} in NiOOH matrices[44]. 8) Both Fe^{4+} and Ni^{4+} are formed upon polarization, and they create a synergism in which the high spin (HS) d_4 Fe^{4+} stabilizes the oxyl radical generated with Ni^{4+} through superexchange contact, while the low spin (LS) d_6 Ni^{4+} promotes the production of O-O[45].

From previous studies, it was not fully cleared that which site is playing an active role in enhancing the activity and how the structure of catalyst evolves during the reaction. This is hampered due to insufficient information about the electronic structure of the composite during the chemical reaction. To observe the electronic and structural changes in the composite

during a redox reaction, Corrigan et al. conducted an *in-situ* ^{57}Fe Mössbauer spectroscopic study[46]. They said that the electronic changes at Fe site are not due to the redox process in Fe, but attributed to the host lattice in a composite material. Moreover, an intimate combination of Fe and Ni on an atomic scale rather than the mixture of $Ni(OH)_2$ and FeOOH particles exhibited better performance for OER rather than either of the single component hydroxides. It was also expected that highly oxidized Fe sites in composite hydroxide may play a key role in OER. Friebel et al. investigated the NiFe oxide structure using *in-situ*/*operando* XAS and concluded that most of the Fe remains in the 3+ oxidation state during the reaction and computational studies by Nørskov et al. implicated Fe^{3+} as the active sites for OER[43]. Moreover, NiFe-based catalyst was investigated at potentials where only Ni^{2+} could be oxidized but not enough to promote OER[46]. And a change observed in ^{57}Fe isomer shift (δ) value from 0.32 to 0.22 mm·s^{-1} was ascribed to transfer of electron density away from Fe^{3+} species upon oxidation of the Ni centers.

The presence of Fe^{4+} in the OER was first clearly observed in 2015 when Stahl et al. investigated NiFe-LDH electrocatalyst during OER[47]. They used *in-situ*/*operando* ^{57}Fe Mössbauer technique to track the Fe oxidation state in 3:1 NiFe-LDH and Fe oxide catalysts, while polarizing them in the OER zone. Interestingly, as shown in Figure 5, the existence of Fe^{4+} was confirmed upon polarization and under OER conditions, which increased with increasing potential. They found that the pure Fe oxide did not show any Fe^{4+} in the OER reaction, demonstrating that Fe^{4+} can only be stable in the NiOOH lattice. This also further illustrated that $Ni_xFe_{1-x}OOH$, in addition to Ni^{4+} generation in the OER reaction, also has Fe^{4+} and that the presence of NiOOH lattice favors the generation of Fe^{4+}. As shown in Figure 5(B), Mössbauer spectrum under open circuit conditions exhibited a doublet with a δ value of 0.34 mm·s^{-1} and quadrupole splitting (Δ) value of 0.46 mm·s^{-1}, and did not show any change at 1.49 V vs. RHE as shown in Figure 5(C) (potential below the onset). At 1.62 V where a significant OER activity recorded, a shoulder peak at δ =

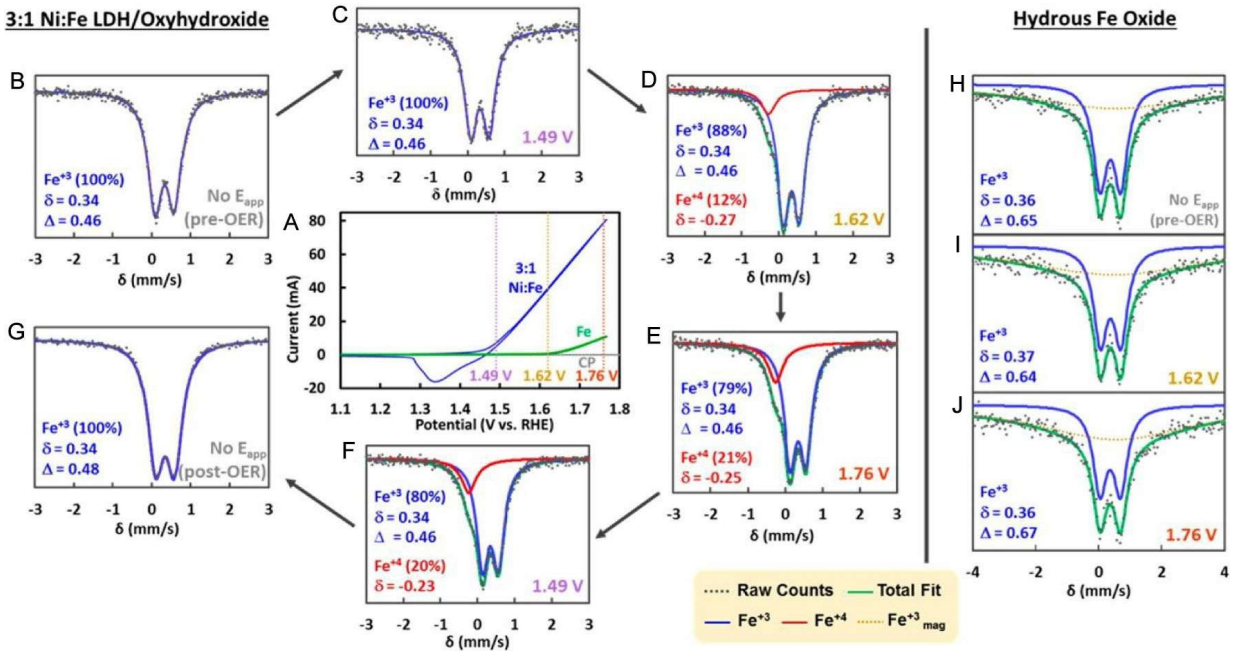

Figure 5 CVs of NiFe layered oxyhydroxide (blue) and hydrous Fe oxide (green) electrocatalysts used for the *in-situ*/*operando* experiments with ^{57}Fe Mössbauer spectra collected at open circuit potential (gray), 1.49 V(purple), 1.62 V(yellow), and 1.76 V(red) vs. RHE. CV data were recorded in the Mössbauer-electrochemical cell with a scan rate of 25 mV·s^{-1} prior to Mössbauer measurements[47]. Copyright©2015. American Chemical Society. Reproduced with permission. (color on line)

-0.27 mm·s^{-1} appeared, which indicates 12% of the Fe sites shown in Figure 5(D). Further increasing the potential to 1.76 V generates a stronger peak for Fe oxidation corresponding to almost 21% of the total Fe (Figure 5(E)). After bringing back the potential to 1.49 V, the current density dropped to baseline, but Fe oxidation peak appeared in Mössbauer spectrum accounting for almost ~ 20% of total Fe as shown in Figure 5(F). After 48 hours without any applied potential, the Fe oxidation peak disappeared (Figure 5(G)).

On the other hand, in the case of ^{57}Fe-enriched hydrous Fe oxide, they did not observe such a behavior in Mössbauer spectra under all the conditions as shown in Figure 5(H-J). And the spectra showed only a doublet (δ = 0.36 ~ 0.37 mm·s^{-1}, Δ = 0.64 ~ 0.67 mm·s^{-1}). The significant feature of NiFe catalyst was the appearance of Fe oxidation peak under an applied potential (> 1.5 V). This new peak was fitted either as a singlet (δ = -0.27 mm·s^{-1}) or as a doublet (δ = 0.0 and Δ = 0.58 mm·s^{-1}), and is consistent with the oxidized Fe species as Fe^{4+}. This was the first direct evidence of the Fe^{4+} formation under reaction conditions. Furthermore, the presence of these Fe^{4+} species even after lowering the potential where the activity dropped to baseline indicated that these species were not directly responsible for the observed activity but playing a key role in enhancing the OER activity. This discovery showed that Fe^{3+} in NiFe-LDH lattice is redox-active under OER conditions and produces highly OER-active Fe^{4+} species. This now explains why Fe exhibits such a significant OER increase when doped to Ni host oxides/hydroxides. Another intriguing result of this research was that no such oxidation occurs when Fe^{3+} is isolated in Fe hydroxide. As a result, a suitable host like NiOOH is required for Fe^{3+} to be redox-active and OER boosting. Therefore, they believed that the stable host lattice of NiOOH is responsible for the production of Fe^{4+}. Because Fe^{4+} species are not anticipated to be identified under the measurement circumstances, they hypothesize that these observed Fe^{4+} species are situated at an interior location in the layer and are surrounded by Ni. And suggested these undiscovered Fe^{4+} species as potential active locations if they exist, but could not give any clear understanding about the role of Fe during OER. XAS results showed that the bond length of Fe-O in NiFe-based catalysts was significantly shorter than that of Fe^{3+}-O, which indicated that Fe should be in higher valence states during the OER process, and supported the results of *in-situ*/*operando* Mössbauer studies[43]. This work gave a strong and clear indication for the existence of high valance iron which surely presents in the system and may have a crucial role in OER, but not much clear. The results of oxygen intermediates study also supported the presence of high-valent iron[48]. However, there is still debate on the mechanism of NiFe catalyst during OER reaction, whether Ni is active sites or Fe is active sites.

Later on in 2018, NiFe Prussian blue analogues (NiFe-PBAs) were studied for OER through *in-situ*/*operando* XAS technique[49]. It was observed that NiFe-PBA was first transformed into $Ni(OH)_2$ and then into $NiOOH_{2-x}$ under the applied potential due to deprotonation, which showed an excellent activity at very low overpotential. They called the deprotonation process a reversible process which partially generated Ni^{4+} as a result of charge compensation due to deprotonation. In other words, *in-situ* generated catalyst $NiOOH_{2-x}$ during OER was considered as responsible for higher activity which can be transformed reversely to $Ni(OH)_2$. This indicated that the structure of the catalyst cannot be stabilized under reaction condition and could be changed by applying potential. In fact, this study gave one clear example about dissociation of catalysts under OER condition for *in-situ*/*operando* spectroscopic characterization which is a major drawback for the *in-situ*/*operando* study.

It is apparent from the above significant findings that there is no clear-cut mechanism, and it is difficult to reach a consensus on how Fe improves the OER activities of Ni-based OECs and what the structure or real phase of catalyst is playing active role in OER, and how it could be stabilized. There are some studies of NiFe-based OECs using *in-situ*/*operando* techniques, but the problems in such studies are that they could not determine the active sites for OER and

failed to fully explain the underlying mechanism for OER. Moreover, we believe that the higher activity is crucial, but it should not be the only concern for any OER catalyst. The stability of the structure under OER conditions is also very important because the stability of the catalyst structure under OER conditions is crucial for commercial applications.

3 The General Introduction of *In-Situ/Operando* Techniques for Characterizing the NiFe-Based OER Electrocatalysts

In the past, traditional electrochemical techniques such as Tafel slopes and electrochemical impedance spectroscopy (EIS) typically offer only indirect and partial information regarding reaction kinetics, making it difficult to deduce the mechanism of OER [50]. Motivated by this challenge, the structural and valence states of the NiFe-based OECs have also been determined using different *in-situ*/*operando* techniques to study the OER mechanism, identify the actual active phase, and demonstrate the functional roles of Fe and Ni during OER[51]. A variety of cutting-edge techniques including Raman spectroscopy, XAS, ambient pressure X-ray photoelectron spectroscopy (APXPS), Mössbauer spectroscopy, UV-visible (UV-vis) spectroscopy, DEMS, and surface interrogation scanning electrochemical microscopy (SI-SECM) were used to monitor the OER process in order to identify reaction intermediates and electrochemical activity on the surface of OECs during the OER[52-53]. These *in-situ*/*operando* techniques can provide information about the structural and electronic states of NiFe-based electrodes. Figure 6 graphically shows several selected *in-situ*/*operando* spectroscopic characterization techniques which have been successfully applied to capture the NiFe-based OER electrocatalytic intermediate species, investigating the OER pathways and mechanism[54].

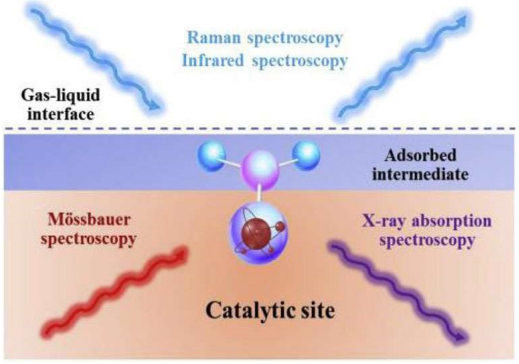

Figure 6 Selected *in-situ*/*operando* spectroscopic characterization techniques for being available to capture the NiFe-based OER electrocatalytic intermediate species, investigating the OER pathways and mechanism[54]. Copyright©2021. Elsevier Inc. Reproduced with permission. (color on line)

Raman spectroscopy could be used to observe vibration, rotational, and other low frequency modes of the NiFe catalysts[55]. The *in-situ*/*operando* Raman spectroscopy could monitor the intermediates during the electrochemical systems under the applying test voltage in aqueous media, which could provide real-time reaction information. This technique helps to understand how an electrochemically driven reaction occurs. The *in-situ*/*operando* XAS could serve as a valuable technique for studying the electronic structure and local geometric structure of catalyst materials under working conditions. The XAS technique includes two regions: X-ray absorption near the edge structure (XANES) and extended X-ray absorption fine structure (EXAFS). Combing with the *in-situ*/*operando* XAS techniques, Friebel et al. found that the $Ni_{0.75}Fe_{0.25}OOH$ catalyst has an α-$Ni(OH)_2$ structure at a low potential and a γ-NiOOH structure at a high potential. With the potential increasing, the shrinkages of the metal-oxygen and metal-metal distances indicate that in α-$Ni(OH)_2$ and γ-NiOOH, Fe has replaced Ni[43]. Moreover, Görlin et al. found that the carbon-supported NiFe catalyst has a larger proportion of Ni^{4+} centers than the non-carbon-supported catalyst via the *in-situ*/*operando* XAS tool. They attributed it to the fact that the electrolyte can more easily contact more OER active centers[38]. The XPS is served as a useful tool for obtaining surface element composition, and chemical oxidation and electronic state of materials. However, due to the need for ultra-high vacuum (UHV), many *in-situ* applications are subject to constrained conditions. APXPS based on

synchrotron radiation can overcome the limitations of UHV conditions[56]. Ali-Lcytty et al. conducted *in-situ* APXPS experiments on NiFe based catalysts under OER conditions. They found that when the electric potential is increased from 0 to 0.3 V (vs. Ag/AgCl), i.e., $Ni(OH)_2$ is oxidized to NiOOH, the O/OH ratio increases significantly. In addition, the Ni and Fe 2p XPS spectra also show the oxidations of Ni and Fe during OER process[57]. The *in-situ*/*operando* UV-vis spectroscopy is used to track the metal oxidation process that occurs in $Ni(OH)_2$. Görlin et al. used *in-situ*/*operando* UV-vis spectroscopy to track the metal oxidation process in NiFe based electrocatalyst. It was found that Fe inhibited the oxidation form Ni^{2+} to $Ni^{3+/4+}$ during the OER process. Combing the *in-situ*/*operando* UV-vis spectroscopy, they concluded that OER was carried out at the center of Ni^{2+} in the NiFe-based catalyst[37]. Moreover, Görlin et al. used *in-situ*/*operando* DEMS to track the Faraday charge distribution from the addition of the catalyst to the product formation and the redox process of the catalyst. The lower metal redox charge indicates that the average valence of Ni in the NiFe-based catalyst is lower than that of nickel oxide catalysts. They concluded that the Fe inhibits the oxidation of Ni during OER and seems to have a stabilizing effect on low valent Ni, thereby promoting OER[37].

Among several other *in-situ*/*operando* techniques, ^{57}Fe Mössbauer spectroscopy is a strong method with very high energy resolution that uses the three main hyperfine interaction parameters of ^{57}Fe δ, Δ, and magnetic hyperfine field (B) to determine the oxidation state, electron spin configuration, symmetry, and magnetic information of Fe centers in materials [58]. Therefore, our focus is not only to investigate the role of Fe in enhancing the OER activity of NiFe-based OECs but also stabilizing and confirming the structure of catalysts during OER through *in-situ*/*operando* ^{57}Fe Mössbauer spectroscopy. We hope that one may better understand how Fe doping/incorporation improves the OER activity of Ni-based OECs and design a better catalyst system for OER in alkaline media, providing new solutions for the further deep study of NiFe-based OER catalysts towards practical applications.

4 Introduction of ^{57}Fe Mössbauer Spectroscopy

Mössbauer spectroscopy has progressively become a standard technique for analyzing catalysis processes soon after Mössbauer effect was discovered[59]. This is unique for revealing the "black box" of catalysis because of its *in-situ*/*operando* application capabilities[60]. The main applications of Mössbauer spectroscopy in catalysis research are: 1) identification of active sites or active phases for catalytic processes; 2) investigation of correlations between catalyst structure and catalytic performance; and 3) characterization of catalysts during reaction activation and deactivation under *ex-situ* and/or *in-situ*/*operando* conditions. There are limited numbers of Mössbauer-active elements such as iron (^{57}Fe), tin (^{119}Sn), antimony (^{121}Sb), gold (^{197}Au), nickel (^{63}Ni), ruthenium (^{99}Ru), iridium (^{191}Ir and ^{193}Ir), and neptunium (^{237}Np) etc., which can be studied using Mössbauer spectroscopy. This limitation is due to several criteria such as suitable lifetime of nuclear excited state, transition energy, easy accessibility, and handling. Among these different elements, ^{57}Fe is the most studied and well-known Mössbauer nuclide.

Mössbauer spectroscopy, which involves the emission of γ-rays from radioactive nuclei and the absorption of these γ-rays by other nuclei of the same element, is a powerful technique for studying materials by measuring the hyperfine interactions that arise from the coupling of nuclear moments with electric and magnetic fields acting on the atomic nucleus. The uses of Mössbauer spectroscopy in catalysis and theoretical concepts have been described before in previous reviews where they mainly focused on physical concept of Mössbauer spectroscopy rather than its applications in catalysis[54, 61-62]. Furthermore, it is yet unclear that which sector is best suited for a certain Fe-based catalyst, as well as the exact function of ^{57}Fe Mössbauer spectroscopy in various catalysis fields. As a result, *in-situ*/*operando* ^{57}Fe Mössbauer spectroscopy is a valuable tool for determining the

link between OER behavior and Fe structural characteristics in Fe-based catalysts during the OER process.

4.1 Principle of Mössbauer Spectroscopy

The Mössbauer effect is the absorption and emission of γ-rays from a recoilless nuclear resonance phenomenon, analogous to the acoustic resonance of two tuning forks with the same frequency $f_s = f_r$ for sender (s) and receiver (r). A nucleus with energy E_e at an excited state (with Z proton and N neutron) undergoes transitions to the ground state with energy E_g by producing γ-rays of energy E_γ. The γ-rays may be absorbed by another nucleus of the same type (identical Z and N) in its ground state, resulting in a transition to the excited state of energy E_e. This phenomenon is called γ-rays recoilless resonance absorption as schematically shown in Figure 7(A). Resonance absorption can only be seen if the emission and absorption lines overlap enough. When γ-rays with energy E_γ are emitted or absorbed in freely moving atom (molecule) of mass m, it undergoes a recoil effect with energy E_R which is many orders of magnitude greater than the natural line-width (Γ), hence resonance is not possible in a freely moving atom or molecule (gas, liquid). As a result, the Mössbauer effect cannot be seen in the presence of freely moving atoms or molecules, such as those in a gaseous or liquid form. Recoilless emission and absorption of γ-rays are conceivable in the solid state, and basically un-shifted transition lines may (at least partly) overlap, resulting in nuclear resonance absorption.

German scientist, Rudolf Ludwig Mössbauer, while he was 27 years old in graduate school, proved this effect experimentally by freezing the source and absorber close to liquid nitrogen temperature, where atoms are firmly bonded in the lattice and the recoil effect is much reduced. Rudolf Ludwig Mössbauer was able to explain this phenomenon using quantum mechanics, demonstrating that atoms as lattice harmonic oscillators do not change their quantum mechanical state upon emission or absorption of γ-rays for a certain probability, which is relatively high for hard and low for soft materials (zero-phonon processes)[59]. Nuclear resonance absorption of recoilless γ-rays, named as Mössbauer effect, soon after he was awarded the Nobel prize in physics 1961, may be detected only for this proportion, known as the Lamb-Mössbauer fraction[63].

Figure 7(A) describes the overall Mössbauer effect phenomena in which the mean lifetime of the excited state of the parent nuclei is very important. For example, the first excited state of ^{57}Co has the mean lifetime of around 100 ns which is normally being used for ^{57}Fe Mössbauer experiment. As a result of the radioactive decays, the excited state of ^{57}Co decays to ^{57}Fe excited state by electron capture process. The excited state of Mössbauer nucleus decays and comes to ground state. The decay of ^{57}Co generates two excited states of ^{57}Fe where almost 99% decay occurs for the lowest energy level which is 14.4 keV and is known as the first excited state from ground state of ^{57}Fe. The ground state of ^{57}Fe does not undergo any kind of decay and the decay constant is zero for it due to zero energy level. Each nuclear level possesses specific energy, spin, parity, and decay constant k mean probability of decay per unit time.

As shown in Figure 7(B), due to the electrical monopole interaction, the electrical quadrupole interaction, and the nuclear Zeeman interaction, the nuclear energy levels of ^{57}Fe (ground and first excited states with nuclear spins of 1/2 and 3/2, respectively) can be split by electric or magnetic fields acting at the nucleus. The hyperfine interactions are able to cause a positive or negative shift of the peak position from zero position of the relative velocity (Doppler velocity), and the shape of the ^{57}Fe Mössbauer spectrum can be changed from a single absorption peak to double and even sextet. In Figure 7(B) schematically shows the shift and splitting of nuclear energy levels and the corresponding ^{57}Fe Mössbauer spectral shape changes when the three kinds of hyperfine interactions are considered solely. In actual samples, the three kinds of hyperfine interactions are often existed simultaneously at iron nuclear positions, and the peak position of the resulting Mössbauer spectrum, the peak spacing and the shape of the Mössbauer spectrum will be more complex.

Usually there are three main parameters obtained from Mössbauer spectroscopy in data form by curve fitting measured Mössbauer spectra, which gives information about electronic, structural and magnetic properties of investigated material include: 1) Isomer shift (δ) arises from Coulombic interaction between the nucleus and the *s*-electrons, 2) quadrupole splitting (Δ) arises from the interaction of electric field gradient with the electric quadrupole moment of the nucleus, and 3) magnetic hyperfine field (B) arises from the interaction between the nuclear magnetic dipole moment and the effective magnetic field at the nucleus. That is, in turn, through the observation of the γ-rays recoilless nuclear resonance phenomenon, the Mössbauer effect, obtaining measured Mössbauer spectrum, analyzing it by considering the various hyperfine interactions existed in the nuclear location, we can study the configuration and distribution of orbital electrons, the physical properties of catalytic material, structural properties and chemical bonding properties, etc.

4.2 ^{57}Fe Mössbauer Instrumentation

A standard Mössbauer spectrometer mainly consists of a radiation source (normally ^{57}Co in a Rh or Pd metal matrix for ^{57}Fe Mössbauer spectroscopy), a velocity transducer, a device for velocity calibration, waveform generator and synchronizer, γ-rays detection system, multichannel analyzer, computer, and an optionally cryostat (low temperature) or oven (high temperature) attached in the setup to control the

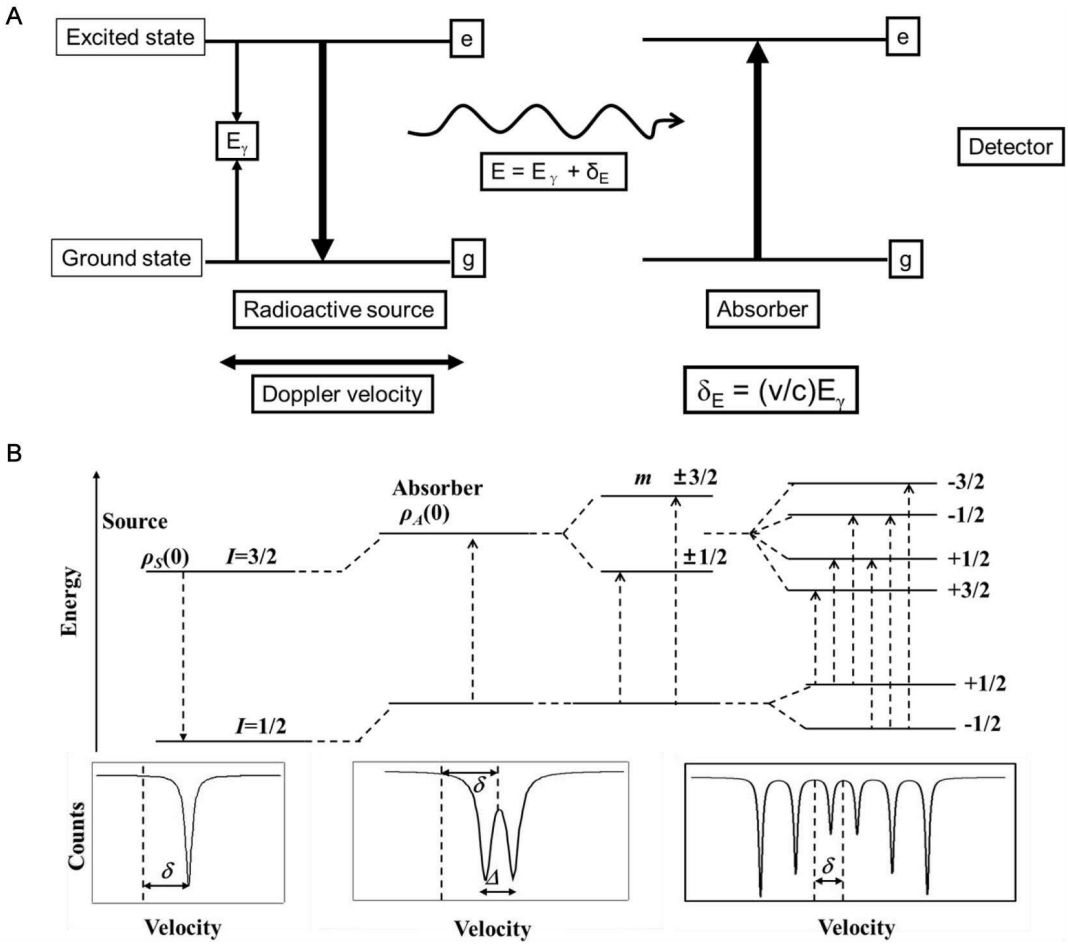

Figure 7 (A) Schematic illustration for emission of specific energy γ-rays from the excited state of nucleus in the Mössbauer source and recoilless γ-rays resonant absorption of the same nucleus in the ground state in the absorber (sample). (B) Nuclear energy levels splitting in case of a transition between I_g = 1/2 and I_e = 3/2 like that of ^{57}Fe due to electric monopole interaction, or electric quadrupole interaction or magnetic hyperfine interaction, and the corresponding ^{57}Fe Mössbauer spectra.

temperature during measurement, which make this instrument suitable to operate at a wide range of temperature conditions. Schematic illustration of (A) configuring a Mössbauer spectrometer and (B) observing modes of a Mössbauer spectrum is shown in Figure 8. In transmission mode as shown in Figure 8(B), an absorber (sample under study) is placed between the source and detector to observe the negative peaks corresponding to absorption of 14.4 keV γ-rays. In backscattering mode, the source and absorber are placed on the same side to observe positive peaks corresponding to absorption of 14.4 keV γ-rays, and the conversion electron Mössbauer spectrum (CEMS) is produced by detecting only the emitted internal conversion electrons by using specific CEMS detector.

Mössbauer spectra are generated by the velocity sweep method in which a moving driver or velocity transducer is used to move the source or sample repeatedly (so-called Doppler moving) with a specific velocity, while γ-rays are transmitted or emitted continuously through the sample and counted on synchronization channels. Usually, the source is mounted on a vibrational axis of an electromagnetic transducer which moves according to voltage waveform applied on the driving coil of the systems, and acceleration with a triangular waveform frequency of this transducer is between 5 ~ 50 Hz. The detecting system is used to detect and store the signal counts in a memory of typically 1024 channels. An external clock subdivides the time intervals of waveform applied to the driven system into number of channels which synchronizes the channel number in the memory and

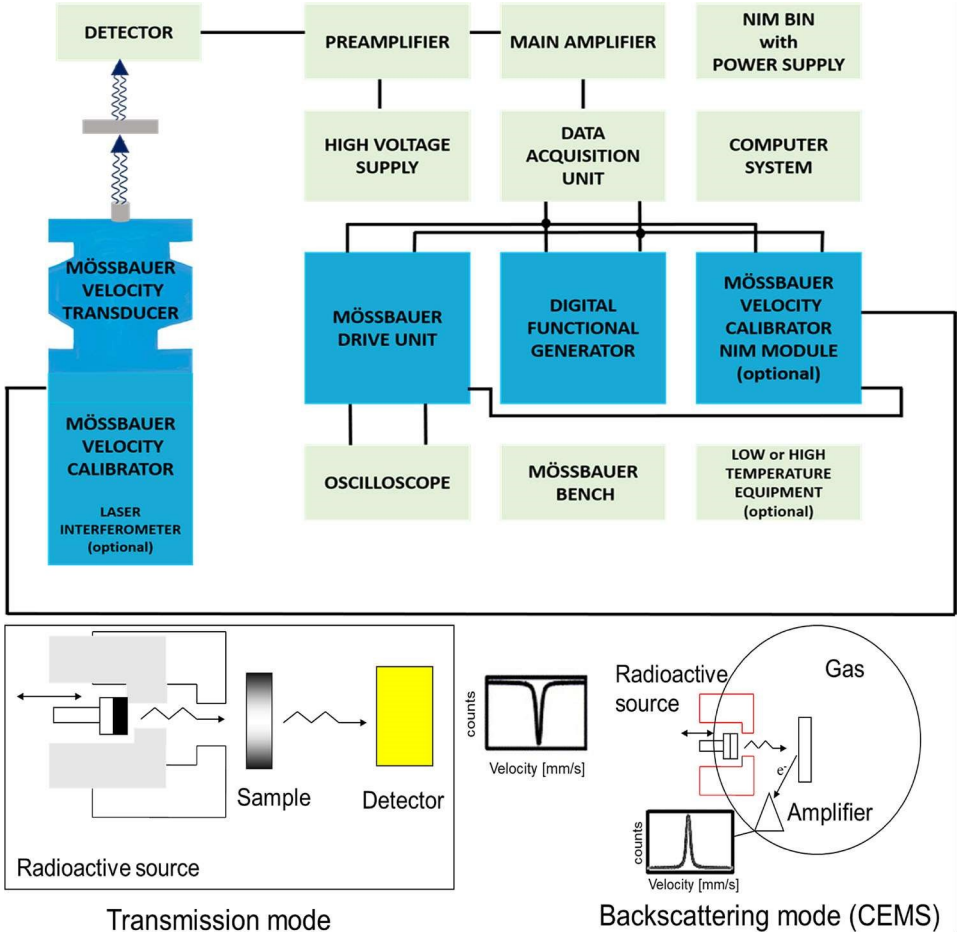

Figure 8 Schematic illustration of (upper part) configuring a Mössbauer spectrometer copied with permission from webpage: http://www.wissel-instruments.de/ and (lower part) Operational modes of Mössbauer spectroscopy for observing a spectrum: Transmission mode (right) and backscattering mode (left, CEMS measurement). (color on line)

instantaneous velocity of the source by advancing memory address one by one. The triangular waveform and 1024 memory channels produce two mirror-imaged Mössbauer spectra each with 512 channels. With sufficiently good velocity linearity, the two spectra can be easily combined (to increase the signal to noise ratio) to give one 512 channel Mössbauer spectrum.

4.3 Data Analysis and Fitting

After obtaining data from experiment, the next step is analysis and fitting of the spectra to determine the active phase structure and valence states of Fe in the catalyst. The fitting of data is usually approximated after comparison with previously available data in the literature or database system. The past data can help in the attribution and screening of the object phase, valence state, spin state and coordination structure based on the analytical and fitted results. Therefore, the database system was developed which is a globally connected network of different centers for Mössbauer effect reference and data. These centers collect data from the Mössbauer analysis of the published literature where it can be used for fitting and analysis of future materials. One of the biggest centers of Mössbauer effect, where the reference and data collected from the whole world for different Mössbauer samples, is Mössbauer Effect Data Center at Dalian Institute of Chemical Sciences, Chinese Academy of Sciences (https://medc.dicp.ac.cn/)[64].

Furthermore, there are several sophisticated methods and software available for analyzing and interpretation of Mössbauer data. Among different types of software available in market, Mosswin is one of the most sophisticated software for data analysis and fitting (http://www.mosswinn.com/)[65]. Fitting methods and model assumptions can have a significant impact on the interpretation of Mössbauer spectra under certain situations due to overlapping of data peaks usually. Therefore, members of a research group use one common software and analysis method for spectral analysis, and any discrepancy in interpretation due to the usage of different programs could be reduced. Mössbauer spectra have been interpreted using different physical models, but only a few of these models have been compared and published.

A variety of physical models are used by the analysis software to produce a model spectrum with which measured spectrum could be compared, fitted, and analyzed. The fitting of the Mössbauer spectrum should not only be carried out on the obtained data, but first also consider a theoretical model. This is because fitting could get superficially unreasonable chi-squared value (χ^2) if based on unphysical model. Commonly, there are three different line shapes employed for modeling of a Mössbauer spectrum as shown in Figure 9. The combination of Lorentzian and Gaussian line resultant is called as the Voigt line shape which is referred to as a pseudo-Voigt function since it is a linear mixture of the two shapes.

Error in analysis is obvious and it varies from laboratory to laboratory. Doublet areas are typically stated to no better than one significant place after the decimal. Isomer shift (δ) and quadrupole splitting (Δ) values are often ± 0.02 mm·s^{-1}, and magnetic hyperfine field (B) values are exceedingly erratic. In general, Mössbauer technique can detect down to 1% of the total normal Fe in the sample, but challenging for the samples containing less than 0.1% weight Fe, the Mössbauer signal is available to be largely enhanced if the enriched isotope ^{57}Fe is used for preparing the samples.

Taking an example of NiFe-(oxy)hydroxide OECs, generally two symmetrical peaks of almost equal height are expected for pre-OER powder-based catalyst, indicating the presence of only one kind of Fe^{3+} species. This kind of spectrum could be simply approximated and fitted with two Lorentzian lines, only one doublet confirms the one kind of Fe^{3+} species in the system. In our work recently published, all spectra of NiFe-(oxy)hydroxide OECs were fitted to Lorenrentzian profiles by the least-squares method, and the fit quality was controlled by the standard χ^2 and misfit tests (MossWinn program)[66].

In this way, the ^{57}Fe Mössbauer spectral parameters could be determined, including the isomer shift (δ), the electric quadrupole splitting (Δ), the full width at

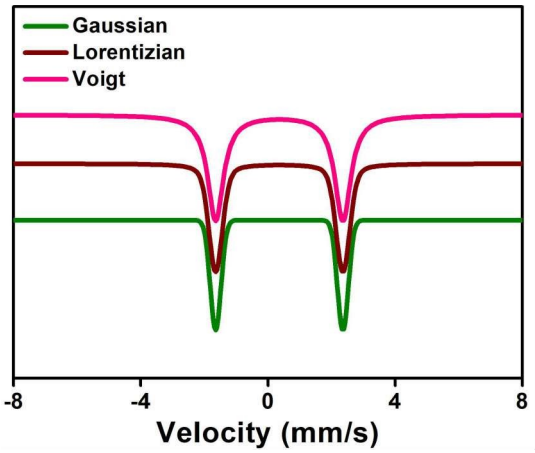

Figure 9 Different line shapes employed for approximation of practically measured ^{57}Fe Mössbauer spectra. (color on line)

half-maximum (Γ_{exp}), and the relative resonance area (A) of the different components of the absorption patterns. In the case of two different kinds of Fe^{3+} species in the system which could arise due to difference in coordination at the surface and inside the lattice, the fitting of the spectrum may not be simple and could require fitting with two doublets or one doublet and one singlet. The presence of high valence Fe such as Fe^{4+} could be confirmed if the spectra could not be fitted with only one doublet and an isomer shift is observed around zero and even negative side. Moreover, stability of catalyst structure can also be confirmed by comparing pre-OER and post-OER spectra by fitting equally. Any difference in the spectra of two states indicates that catalyst structure is not stable and phase changes might occur which could create ambiguity about the final results. Therefore, it is strongly recommended that *in-situ*/*operando* study is conducted for the catalyst which does not undergo any kind of structural transformation under applied potential or during OER.

5 *In-Situ*/*Operando* Mössbauer Spectrometer Setup for OER Study

Mössbauer spectroscopy becomes very important tools for the characterization of NiFe-based OECs since a very small amount of Fe significantly enhances the OER activity of these materials. Later in the 1980s, it was received a huge attention to the research on electrochemical water splitting processes utilizing non-precious metal oxides and hydroxides to replace the precious metal ones and costly anodic materials. Corrigan conducted one of the significant researches in which he discovered that when Fe impurities are injected into NiO anodes, the OER activity increases[32]. Afterward, several other transition metal cations were investigated for their impact on OER performance by impregnating into NiO electrodes[35]. But not a comparable OER-enhancing impact was observed from any other *d*-block element except Ce^{4+}, which showed similar improvement in OER activity of NiO. Nonetheless, the degree of Ce^{4+}-induced enhancement was near to that of Fe^{3+}-induced enhancement. However, until 2014-2015, no significant effort was made to give a logical and acceptable explanation for this enhancement. And for more than two decades, these findings of Fe impurities-based enhanced OER performance of Ni-based materials were completely hidden.

Since Mössbauer study of NiFe-OECs provided some reasonable explanations to this unprecedented OER activity, it became crucial to develop and improve the *in-situ*/*operando* Mössbauer electrochemical setup and experimental understandings. Firstly, we discuss the key challenging issues and parameters to develop an *in-situ*/*operando* Mössbauer instrument for OER reaction to observe the evolution of the chemical state of the iron dynamically in the catalyst and structure of the catalyst during electrochemical reactions. The *in-situ*/*operando* setup consists of ^{57}Fe Mössbauer spectrometer connected with electrochemical station to conduct electrochemical reactions and Mössbauer analysis simultaneously. A typical *in-situ*/*operando* Mössbauer electrochemical setup, which was self-developed in our lab, is shown in Figure 10 (D). This setup consists of three main parts: 1) Mössbauer spectrometer, 2) electrochemical station, and 3) locally designed *in-situ*/*operando* OER electrochemical reaction cell. In our lab, we use single line ^{57}Fe Mössbauer radiation source ^{57}Co(Rh) with 14.4 keV level γ-rays, which could reduce attenuation in electrolyte and obtain a satisfactory signal-to-noise ratio

attached with CHI660E electrochemical station. The Doppler velocity of the spectrometer is calibrated with respect to α-Fe at 298 K according to the international recommended standardization. Generally, before the *in-situ/operando* OER characterization experiment, the electrolyte is saturated with nitrogen or argon to remove the dissolved oxygen. Therefore, accessories such as a gas cylinder are added as shown in Figure 10(D).

We have self-developed several kinds of *in-situ/operando* electrochemical reaction cells for ^{57}Fe and ^{119}Sn Mössbauer spectral measurements using one kind of commercialized Teflon material without containing any iron impurity, which is a cheap, stable, and easily machined material with very low γ-ray absorption property. An electrochemical reaction cell with high versatility for *in-situ/operando* Mössbauer spectral measurements is shown in Figure 11. Very thin windows of about ~ 0.6 mm thickness with the diameter of about ~ 10 mm aligned with the source and detector were carved into both walls of the working electrode area for the facile passage of γ-rays. The distance of the two windows was only a few millimeters to reduce the attenuation of γ-rays and enough to immerse 3 ~ 5 pieces of working electrodes parallel to each other with a distance of less than 1 mm. Two small peristaltic pumps, such as NKCP-S04B type model, can be connected with the

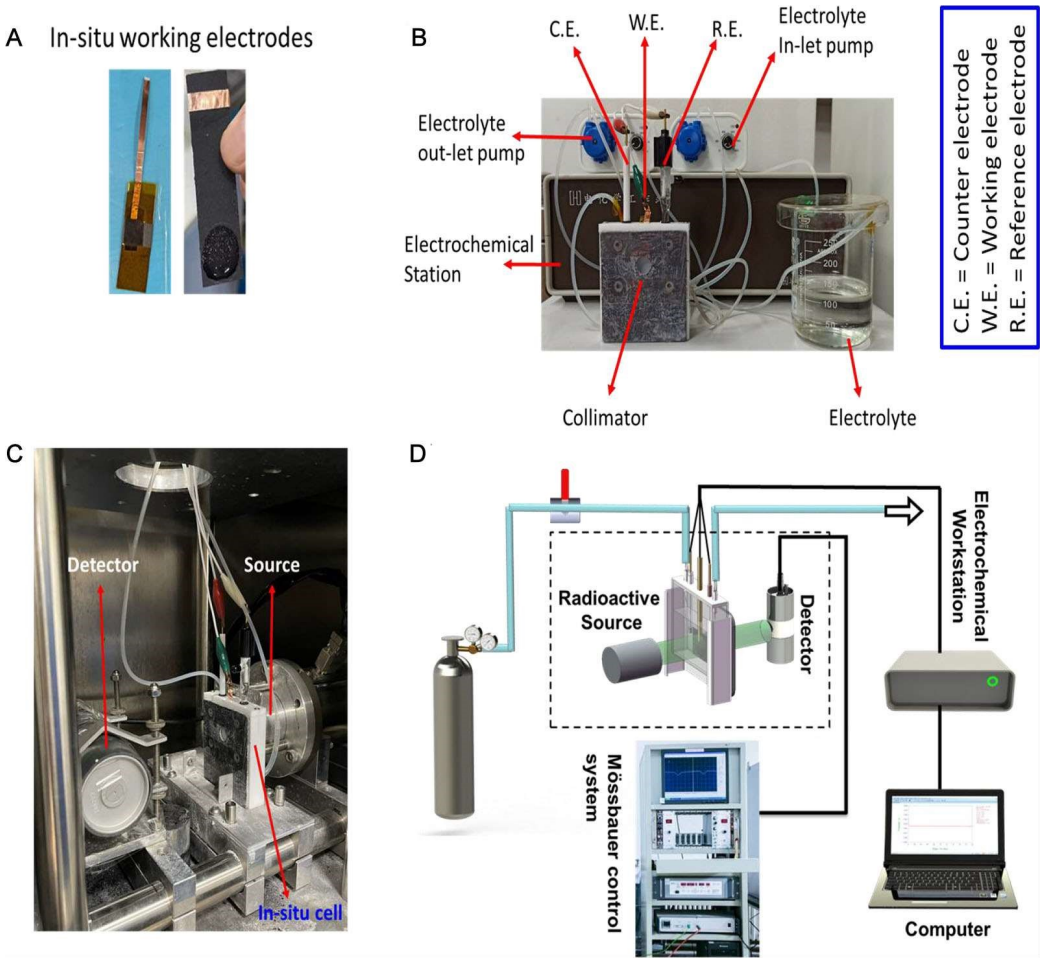

Figure 10 (A) Fabricated electrodes for *in-situ/operando* Mössbauer-electrochemical test. (B) A front view of self-designed Mössbauer-electrochemical reaction cell connected with electrochemical station. (C) *In-situ/operando* Mössbauer-electrochemical cell placed inside the Mössbauer instrument ready for coinstantaneous OER reaction and Mössbauer measurement. (D) The schematic illustration of *in-situ/operando* electrochemical ^{57}Fe and ^{119}Sn Mössbauer setup for electrochemical OER characterizations[66]. Copyright©2021. ELSEVIER B.V. Reproduced with permission. (color on line)

reaction cell where the electrolyte enters from lower part of reference electrode and after passing through working electrode area leaves from upper side of counter electrode. This kind of flow style can help to maintain the pH during the electrochemical reaction. The flow rate of both pumps keeps same during the reaction and the amount of electrolyte in a beaker should be enough such as 100 ~ 200 mL to maintain the pH of 0.1 mol·L^{-1} KOH solution.

The fabrication of electrode for *in-situ/operando* Mössbauer test is very sensitive task and needs high attention. For this purpose, the key step is to prepare ink of the catalyst. In a typical OER experiment in our lab, 10 mg of catalyst powder is added into solution containing 40 μL Nafion, 480 μL isopropanol, and 480 μL deionized water in a 5 mL plastic vial. The suspended solution of catalyst is kept in sonication for six hours to obtain a uniform slurry which is important for uniform and stable deposition of catalyst on substrate. The catalyst ink must be evenly coated on substrate such as carbon paper or carbon foil before the test and a conductive copper foil is connected with the substrate as shown in Figure 10(A). A front view of self-designed Mössbauer-electrochemical reaction cell connected with electrochemical station is shown in Figure 10(B). Figure 10(C) is a picture of the *in-situ/operando* Mössbauer-electrochemical cell placed inside the Mössbauer instrument ready for coinstantaneous OER reaction and Mössbauer measurement. A lead plate with 3 mm thickness, with a window of the same size as the *in-situ/operando* cell, is pressed to the cell's front, ensuring that the Mössbauer γ-rays only can enter from the cell's window, and the Mössbauer γ-rays in other directions are shielded by the lead plate. We call this specific lead plate a Mössbauer spectrometer collimator.

Generally, 5 ~ 10 mg Fe cm^{-2} of absorber thickness is recommended in case of normal iron containing substance used in catalyst preparation for a conventional ^{57}Fe Mössbauer spectra measurement, in which the ^{57}Fe nucleus, one kind of the Fe isotopes with only ~ 2.2% natural abundance. For the *in-situ/operando* electrochemical ^{57}Fe Mössbauer testing, the catalyst is recommended to be prepared using enriched ^{57}Fe isotopes for enhancing the resonant absorption signals. Compared with the window material and the carbon paper substrate, the electrolyte solution is the greatest affecting the Mössbauer γ-rays, so, the distance between the two windows of the reaction cell should be as close as possible to be minimized. This is also the main reason for the recommended use of enriched ^{57}Fe isotopes for electrocatalyst preparation. Generally, the enriched ^{57}Fe isotopes can be purchased on the market, the purity is basically 95% and above, which is provided in the form of metallic iron foil or iron oxide. It can be dissolved in a medium such as hydrochloric acid, nitric acid or sulfuric acid, and prepared into the corresponding salts as stock solution for use.

It is well-known fact that only a small amount of

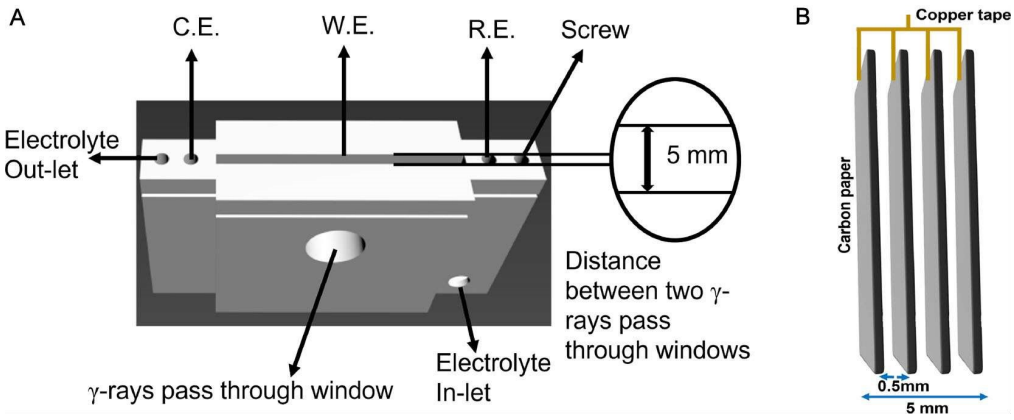

Figure 11 (A) A schematic diagram of self-designed *in-situ/operando* ^{57}Fe and ^{119}Sn Mössbauer electrochemical reaction cell. (B) A schematic illustration of multiple working electrodes parallel arrangement inside the reactor. (color on line)

catalyst is needed for one OER test, but for the *in-situ*/*operando* ^{57}Fe Mössbauer studies enough Fe content in the catalyst is required to detect good quality signals. Depositing a too thick catalyst layer on one working electrode is not recommended as only surface particles will take part in OER while the bottom particles may not take part, hence signals could be mixture of unreacted and reacted Fe in OER catalyst. Therefore, to make it sure that every particle of the catalyst is taking part in OER, and enough amount of catalyst is presented to detect signals, we need several pieces of well-prepared working electrodes placed parallel to each other as shown in Figure 11(B) (3 ~ 5 pieces of electrodes deposited with the same catalyst ink placed at the distance of less than 1 mm). This will facilitate every particle of the catalyst to take part in the OER reaction and enough amount of Fe content to detect good quality signals.

On the other hand, we prefer a continuous flow of electrolyte rather than changing electrolyte after some time as using a small amount of electrolyte and highly active electrocatalyst may result in change of pH of the electrolyte which could alter the reaction dynamics. Hence, a continuous flow of electrolyte through reactor will prevent this kind of pH from changing during the reaction even at longer run. And at the same time, also enough amount of electrolyte must be presented inside the reaction cell during the flow process but only at counter and reference electrode sites, while the working electrode should have very less amount only to make sure electrolyte contact with the catalyst for reaction so that a good quality of signals could be obtained to study briefly. The formation of bubbles on the electrode surface is inevitable during OER especially at higher potential, which could affect the signal quality, so using multilayers of catalyst and exposure to limited amount of electrolyte could largely suppress this problem but not completely.

The electrochemical tests should be conducted in a systematic manner such as first pre-OER should be conducted for catalyst powder without substrate. Then after depositing the catalyst powder on the substrate to study the effect of substrate because if there is any effect we should consider during analysis and fitting process to normalize. After pre-OER tests, first *in-situ*/*operando* test should be conducted at open circuit potential (OCP) to study the effect of electrolyte. Usually, the absorption of γ-rays or strength of the signals could be decreased in the presence of electrolyte, but this problem could be lessened if experiment continues for longer time. Next, one test should be conducted at an applied potential lower than the potential required for OER, i.e., lower than the onset potential. This will show whether there is any change of electrochemical state of Fe species at lower potentials or not. After these initial experiments, now we can go for onset potentials and higher potentials. After studying at different potentials, one should test the post-OER immediately after taking out the electrolyte and removal of applied potentials, and then after 48 hours to 72 hours when the electrode is fully dried. This will give a clear understanding about the structure stability and time required for recovering the original structure capability of the catalyst. If the pre-OER and post-OER spectra of a catalyst are similar and show symmetric, then it could be considered that the catalyst has a stable structure and does not undergo any structural transformation, and the role of the chemical state change of Fe species could also be confirmed under OER catalyst working conditions. One most important point here is that the current density must be stable during whole reaction at every applied potential, which will not only confirm the catalyst stability but also help in determining the real structure of the catalyst.

6 *In-Situ*/*Operando* ^{57}Fe Mössbauer Spectroscopic Study Case

As we have discussed above that presence of Fe^{4+} was first time observed by Stahl et al. but they could not completely explain the role of high valence state of Fe in the OER[47]. And it was assumed that this high valence Fe either plays a direct role as an active site during OER or it enhances the activity of Ni sites. Later on, *in-situ*/*operando* XANES study of NiFe-PBAs indicated that NiFe-PBAs were trans-

formed to $NiOOH_{2-x}$ during OER, which generate Ni^{4+} hence the OER activity was improved. These contradictory and incomplete claims indicated two major flaws in these studies: 1) the real role of Fe^{4+} could not be clearly understood and explained and 2) the reversible structural transformation of NiFe-OECs during the OER, making it unclear that which phase of NiFe-OECs is responsible for higher OER activity. Therefore, we tried to solve both these challenging issues and address well in our following studies.

We have so far discussed the effects of doped/incorporated Fe in Ni-based OECs, their activities, possible factors responsible for higher activity. But it is important to highlight the suitable method for their synthesis and *in-situ*/*operando* studies. We here recommend a suitable and facile method for the synthesis of NiFe-(oxy)hydroxide OECs by using PBAs as precursors, which was newly developed in our lab[67]. We know that PBAs have the typical chemical formula $A_lM_n[\acute{M}m(CN)_6]\cdot xH_2O$, where A indicates the alkali metal ions such as Na^+ and K^+ etc., while M and Ḿ represent the transition metal cations[68,69]. In the PBAs crystal structures, cyanide groups serve as bridges between transition metal ions (M^{2+}–C≡N–M^{3+}). Due to the difference in electronegativities of C and N, the corresponding M and Ḿ metals show high and low spin states, respectively. These materials are useful for different applications such as batteries, gas storage, catalysis, energy storage, sensors, drug delivery, and environmental cleaning[69]. One of the most promising applications of these materials is the use of these materials as a precursor for the synthesis of inorganic nanostructures[70]. It is now possible to synthesize volumes of PBAs with specified compositions and morphologies. PBAs have also gained attention due to diverse and tunable morphologies and sizes. But effective and beneficial use of PBAs mainly depends on processing and synthesis steps to control shape, composition, and size according to the desired application.

6.1 NiFe-PBAs/Carbon Nanotubes OER Electrocatalysts

In first part of our case study here, the structural stability issue of NiFe-OEC was investigated and the real phase of the catalyst was confirmed during OER before going for *in-situ*/*operando* Mössbauer study to further elucidate and understand the mechanism. For this purpose, composites of NiFe-PBAs/carbon nanotubes (CNTs) with the optimized amount of CNTs were synthesized and their OER activities were compared with that of NiFe@C obtained from high-temperature pyrolization of NiFe-PBAs. The NiFe-PBAs/CNTs OER activity with the optimum amount of 8wt.% of CNTs was found to be significantly superior to NiFe@C as shown in Figure 12(A), and the Tafel slope showed the smallest value of 83 $mV\cdot dec^{-1}$ among other samples as shown in Figure 12(B). The X-ray diffraction (XRD) results before and after deposition and activation by CV of NiFe-PBA/CNTs (8wt.%) on carbon paper indicated that the crystal structure was changed after activation as shown in Figure 12(C). The XRD peaks intensities were significantly reduced after activation, which suggests that the crystal structure of NiFe-PBAs was broken during the activation process. The characteristic peaks representing NiFe-PBAs completely disappeared after 125 cycles, indicating that the NiFe-PBA structure had been completely transformed into other structures.

The XRD results after the 500 cycles were similar to 125 cycles, which suggests that there is no further change in crystal structure after 125 cycles. Furthermore, *ex-situ* ^{57}Fe Mössbauer spectral measurement shown in Figure 12(D) before and after activation of NiFe-PBAs showed that after activation no resonance absorption signal could be observed, which proved that the iron cyanide large anions had been completely dissolved into the electrolyte during the reaction and the structure no longer belonged to NiFe-PBAs. This was further confirmed by *ex-situ* and *in-situ*/*operando* Raman spectra as shown in Figure 12(E-F), which exhibited the same results. Hence, the dissociation of $[Fe(CN)_6]^{3-}$ after activation indicated the formation of new Ni-O stretching vibration band which belongs to $Ni(OH)_2$/NiOOH. Therefore, this study revealed that NiFe-PBAs/CNTs OER catalysts will completely undergo dissociation of $[Fe(CN)_6]^{3-}$ upon elec

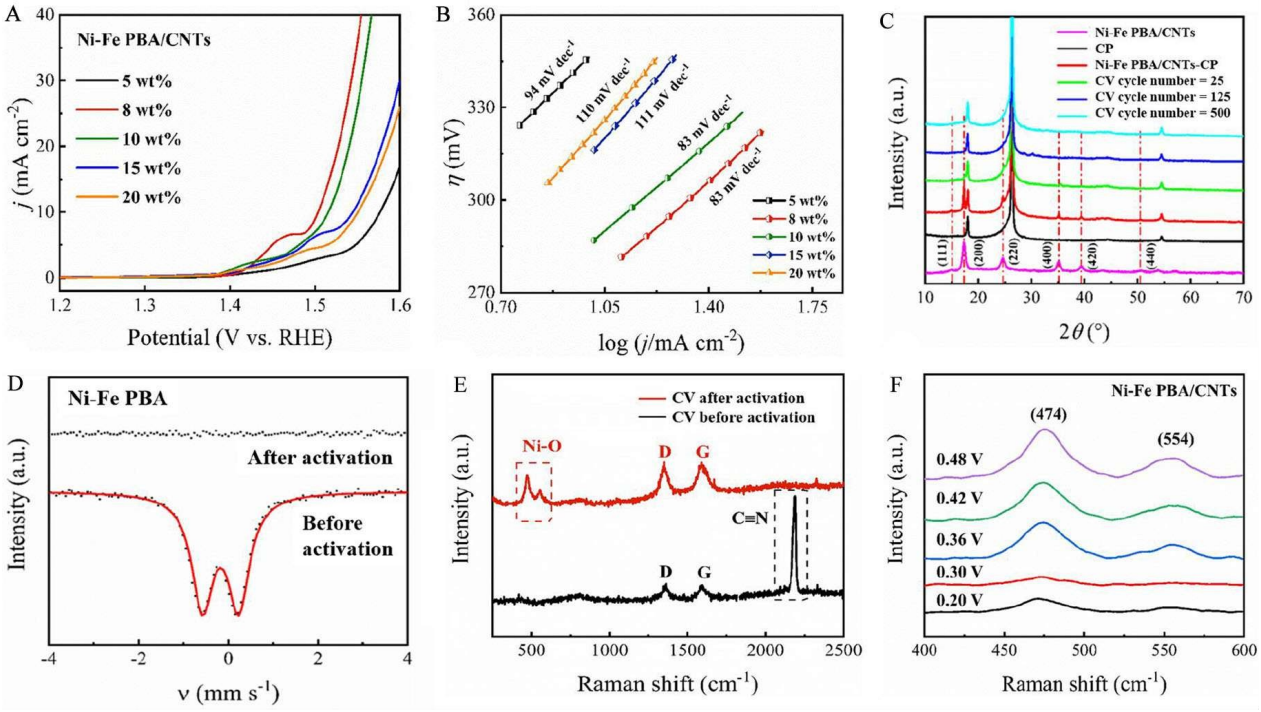

Figure 12 (A) Linear sweep voltammetric results of NiFe-PBAs/CNTs with varying amount of CNTs. (B) Tafel slopes for NiFe-PBAs/CNTs. (C) XRD analysis showing the structures of NiFe-PBAs/CNTs, carbon paper, NiFe-PBAs/CNTs/carbon paper, and NiFe-PBAs/CNTs/carbon paper after activation through cyclic voltammetry. (D) *Ex-situ* ^{57}Fe Mössbauer spectroscopic analysis of NiFe-PBAs/CNTs before and after CV activation. (E) Raman spectra for NiFe-PBAs/CNTs before and after CV activation. (F) *In-situ*/*operando* Raman spectroscopic analysis for NiFe-PBAs/CNTs at different applied potentials. (color on line)

trochemical activation in the alkaline condition generating $Ni(OH)_2$/NiOOH. In this stage, this $Ni(OH)_2$/NiOOH can be considered to the real active phase, which is more reasonable to claim that why NiFe-PBAs has high activity in the OER.

6.2 $NiFe_m$-Fe PBAs Derived $NiFe_m$-(Oxy) Hydroxides OER Electrocatalysts

In the first part of our case study above, we confirmed that the spontaneous dissociation of the NiFe-PBAs in the alkaline solution generated $Ni(OH)_2$/NiOOH, serving as potential and stable structures which do not undergo any kind of further transformation under the applied potential once it is generated. In addition, we previously developed a novel and scalable strategy, containing a "copolymer-co-morphology" conception, to compositionally control synthesis of various types of PBAs which can be topotactically derived into corresponding double oxides[68]. Therefore, a series of $NiFe_m$-(oxy)hydroxides ($NiFe_m$-O_xH_y, m refers to the atomic ratio of Fe/Ni) catalysts were synthesized by the topotactic transformation of $NiFe_m$-Fe PBAs in an alkaline solution. The $NiFe_m$Fe PBAs materials with different iron contents doped in the Ni sites were prepared by our previously developed strategy[71].

One of the novelties in our second part case study here is the topotactic transformation of $NiFe_m$-Fe PBAs into $NiFe_m$-O_xH_y. It was observed from the *ex-situ* ^{57}Fe Mössbauer analysis of $NiFe_m$-Fe PBAs that there are two kinds of Fe^{3+} with different spin states in the system. This indicates that two different Fe^{3+} species are on two different crystallographic positions and all the spectra could be reasonably fitted with two doubles as shown in Figure 13(A-D). The relevant amount of different kinds of Fe^{3+} in every sample containing different amounts of Ni/Fe ratio is given in Table 1. The sensitivity of ^{57}Fe Mössbauer spectroscopy is so high that it could even differentiate

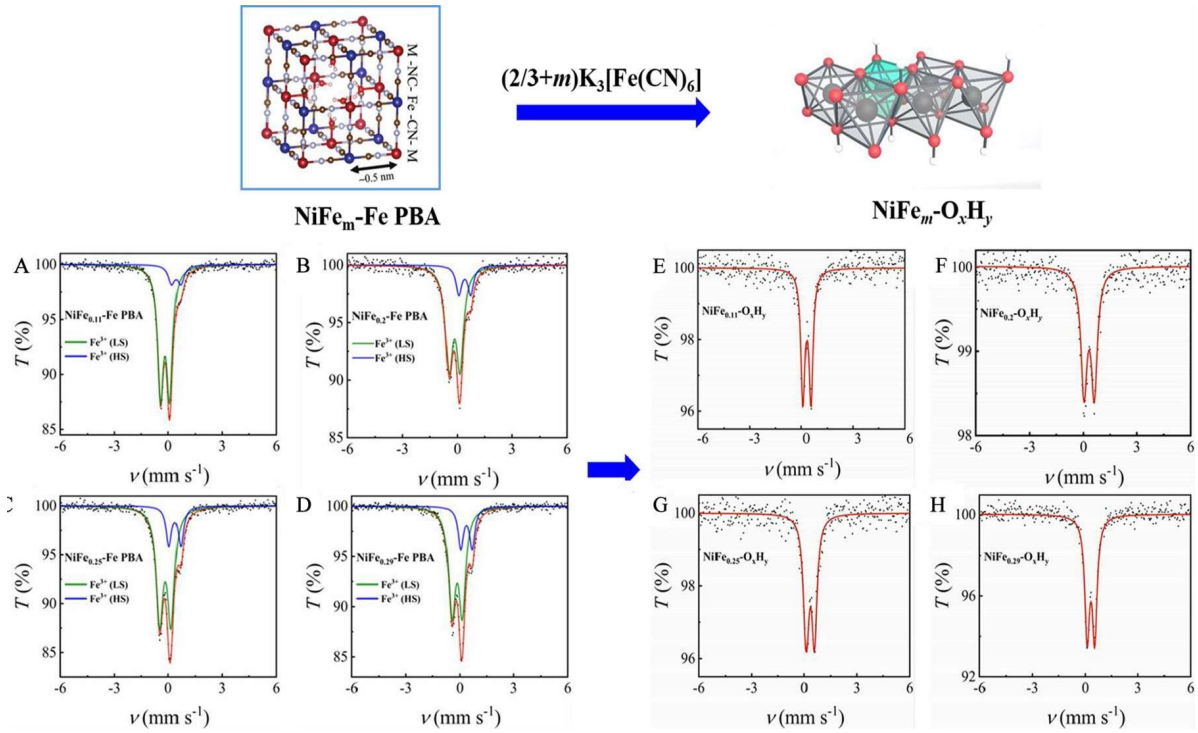

Figure 13 (A-D) *Ex-situ* ^{57}Fe Mössbauer analysis of NiFe$_m$-Fe PBAs doped with different ratios of Ni:Fe. (E-H) *Ex-situ* ^{57}Fe Mössbauer analysis of NiFe$_m$-O$_x$H$_y$ derived from the precursors NiFe$_m$-Fe PBAs by topotactic transformation. (color on line)

between two different crystallographic positions of Fe^{3+} which is usually not possible with other characterization techniques. This makes ^{57}Fe Mössbauer spectroscopy more sophisticated and sensitive to study Fe containing materials. Moreover, increasing the Fe ratio increases the Fe^{3+} amount in the Ni sites, which, later on, will be transformed into NiFe$_m$-O$_x$H$_y$ after treatment with KOH. Interestingly, only one type of high spin Fe^{3+} was observed in *ex-situ* ^{57}Fe Mössbauer analysis for NiFe$_m$-O$_x$H$_y$, and increasing Fe doping without further influence on the one doublet spectral shape and parameters as shown in Figure 13 (E-H) and also listed in Table 2.

Figure 14(A) shows that the NiFe$_{0.2}$-O$_x$H$_y$ exhibited a significant decrease in onset potential after activation through 100 cycles of CV where phase changes occurred from α-phase Ni(OH)$_2$ structure to γ-phase NiOOH structure. *Ex-situ* ^{57}Fe Mössbauer analysis shows a negligible change in the δ values, but there were significant changes in the Δ values before and after electrochemical activation as shown in Figure 14(B-C). Iron has the coordination structure of 6-oxygen coordinated octahedral in both crystal phases of α-phase Ni(OH)$_2$ and γ-phase NiOOH, with smaller Δ value indicating the octahedral symmetry should be higher in later one than the former one. This also further illustrates the high energy resolution of the ^{57}Fe Mössbauer spectroscopic technique where even subtle changes in the electron density and the electric field distribution at the iron nuclide position can be clearly identified. Similar trend was also observed in *ex-situ* and *in-situ*/*operando* Raman spectra where peak shifting and significant rise in peaks intensity were observed after activation as shown in Figure 14 (D-E). The LSV results for different NiFe$_m$-O$_x$H$_y$ catalysts shown in Figure 14(F-G) indicate that NiFe$_{02}$-O$_x$-H$_y$ exhibited the lowest overpotential of 263 mV at the current density of 10 mA·cm^{-2} and the Tafel slope with a value of 35 mV·dec^{-1} was observed (Figure 14 (H)). The catalyst NiFe$_{0.2}$-O$_x$H$_y$ showed a great stability for 100 hours while exhibiting the current density of 100 mA·cm^{-2}.

In summary, in the second part of our case study work, the high-performance OER catalyst of NiFe-

Table 1 *Ex-situ* ^{57}Fe Mössbauer spectral parameters of $NiFe_m$-Fe PBAs at room temperature

Sample	Valence/spin state	δ/Fe (mm·s^{-1})	Δ (mm·s^{-1})	Γ_{exp}(mm·s^{-1})	A (%)
$NiFe_{0.11}$-Fe PBA	Fe^{III} high spin	0.44	0.50	0.43	14
	Fe^{III} low spin	-0.17	0.50	0.38	86
$NiFe_{0.2}$-Fe PBA	Fe^{III} high spin	0.40	0.65	0.38	19
	Fe^{III} low spin	-0.16	0.59	0.46	81
$NiFe_{0.25}$-Fe PBA	Fe^{III} high spin	0.37	0.65	0.34	21
	Fe^{III} low spin	-0.15	0.62	0.45	79
$NiFe_{0.29}$-Fe PBA	Fe^{III} high spin	0.37	0.64	0.36	24
	Fe^{III} low spin	-0.15	0.57	0.44	76

Table 2 *Ex-situ* ^{57}Fe Mössbauer spectral parameters of $NiFe_m$-O_xH_y at room temperature

Sample	Valence/spin state	δ/Fe (mm·s^{-1})	Δ (mm·s^{-1})	Γ_{exp} (mm·s^{-1})	A (%)
$NiFe_{0.11}$-O_xH_y	Fe^{3+} high spin	0.32	0.44	0.28	100
$NiFe_{0.2}$-O_xH_y	Fe^{3+} high spin	0.32	0.58	0.42	100
$NiFe_{0.25}$-O_xH_y	Fe^{3+} high spin	0.34	0.35	0.36	100
$NiFe_{0.29}$-O_xHy	Fe^{3+} high spin	0.32	0.43	0.33	100

(oxy)hydroxides ($NiFe_m$-O_xH_y) was firstly developed through the topotactic transformation of $NiFe_m$-Fe PBAs in an alkaline solution. Furthermore, the phase purity and stability were thoroughly confirmed by *ex-situ* and *in-situ*/*operando* Raman and *ex-situ* ^{57}Fe Mössbauer spectroscopies in combination with other several kinds of conventional techniques. It is indicated that phase structure of $NiFe_{0.2}$-O_xH_y was irreversibly transformed from α-$Ni(OH)_2$ to γ-NiOOH by applying an anodic potential which is different from that of previous report mainly obtain ing from *in-situ*/*operando* XAS characterizations[49]. The amount of Fe was optimized, and the excellent OER electrochemical activity and stability were also demonstrated. That is to say, these catalysts are confirmed to be more stable with no changes into any other structure once it is generated after CV activation.

After making clear the stability issues, the $NiFe_{0.2}$-O_xH_y catalyst with the optimized iron proportion was selected to probe the reaction mechanism of $NiFe_m$-O_xH_y OER electrocatalyst using the self-developed *in-situ*/*operando* electrochemistry Mössbauer characterization instrument as shown in Figure 10(D)[66]. This instrument has also been applied in ORR[72] and CO_2RR[73], which provides a high level of research tool for the preparation of highly efficient catalysts of electrolytic water, carbon dioxide reduction, fuel cell development and even for detecting the structural and electronic properties of single atom catalysts[72,73]. The identifications of durable and non-durable FeN_x sites in Fe-N-C materials for PEMFCs towards practical applications have also been successfully investigated, and the results will be published soon as like that reported by the well-known French team[74].

The *in-situ*/*operando* ^{57}Fe Mössbauer results indicated that Fe was only in 3+ oxidation state in $NiFe_{02}$-O_xH_y at lower applied potentials, such as 1.22 V and 1.32 V, and the spectral shapes are almost the same as the one collected at the open circuit voltage (OCV) as shown in Figure 15(A), where only one doublet is observed with the equal intensity of the two peaks and can be ascribed to high spin Fe^{3+}. However, as the applied potential increased and reached to 1.37 V, the intensity of the two peaks began

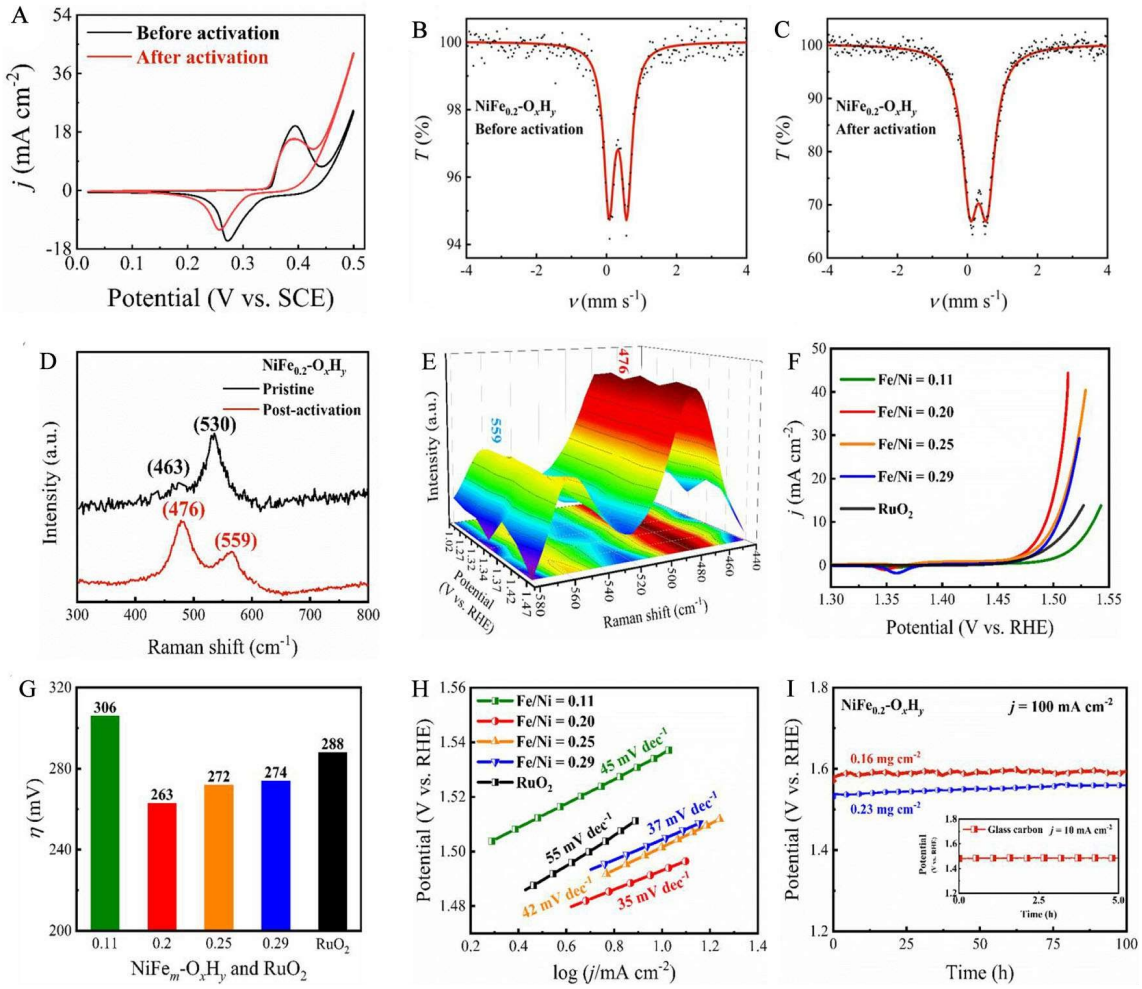

Figure 14 (A) Cyclic voltammetric curves of $NiFe_{0.2}$-O_xH_y before (the black curves, α-phase $Ni(OH)_2$ structure) and after electrochemical activation (the red curves, γ-phase NiOOH structure). (B-C) ^{57}Fe Mössbauer spectra of $NiFe_{0.2}$-O_xH_y before and after electrochemical activation. (D) Raman spectra of $NiFe_{0.2}$-O_xH_y before (black) and after (red) applying anodic potential. (E) Operando Raman spectra of $NiFe_{0.2}$-O_xH_y collected at different applied potentials (V vs. RHE). (F) The OER polarization curves with i_R correction. (G) Overpotentials at 10 mA·cm^{-2}. (H) Tafel plots of $NiFe_m$-O_xH_y with different molar ratios of Fe/Ni and commercial RuO_2. (I) Chronopotentiometric curves of $NiFe_{0.2}$-O_xH_y on Ni foam with different catalyst loadings at a constant current density of 100 mA·cm^{-2} for 100 h. The inset shows the chronopotentiometric curve of $NiFe_{0.2}$-O_xH_y at a constant current density of 10 mA·cm^{-2}[66]. Copyright 2021. ELSEVIER B.V. Reproduced with permission. (color on line)

to become unequal, and a small shoulder peak started to develop with the δ value of around -0.25 mm·s^{-1} as shown in Figure 15(B) which can be attributed to Fe^{4+}[47]. The observed spectral shape has been changed more significantly, indicating that the content of Fe^{4+} further increases as the applied anode potential increases (Figure 15(C-D)). The amount of Fe^{4+} further increased to ~ 40% as the applied potential reached 1.57 V as shown in Figure 15(E). And after that Fe^{4+} completely disappeared as the applied potential was removed, indicating the crucial role of Fe^{4+} species in OER (Figure 15(F)). The pre-OER and post-OER spectra were similar, which indicates the excellent structure stability of the catalyst. The stability was also confirmed through measurement of current density which remained stable throughout the *in-situ*/*operando* Mössbauer measurements (Figure 15(G)). Moreover, combining with the cyclic voltammetric curves (Figure 15(H)), the generation of Fe^{4+} (~ 12% in total) was also observed at around the onset potential 1.42 V vs.

RHE of OER (Figure 15(C)). As listed in Table 3, it is different from the previous *in-situ*/*operando* Mössbauer tests, in which Fe^{4+} was observed at a higher potential rather than around onset potential[47]. Therefore, the *in-situ* produced abundant Fe^{4+} at onset potential and different applied potentials suggested that

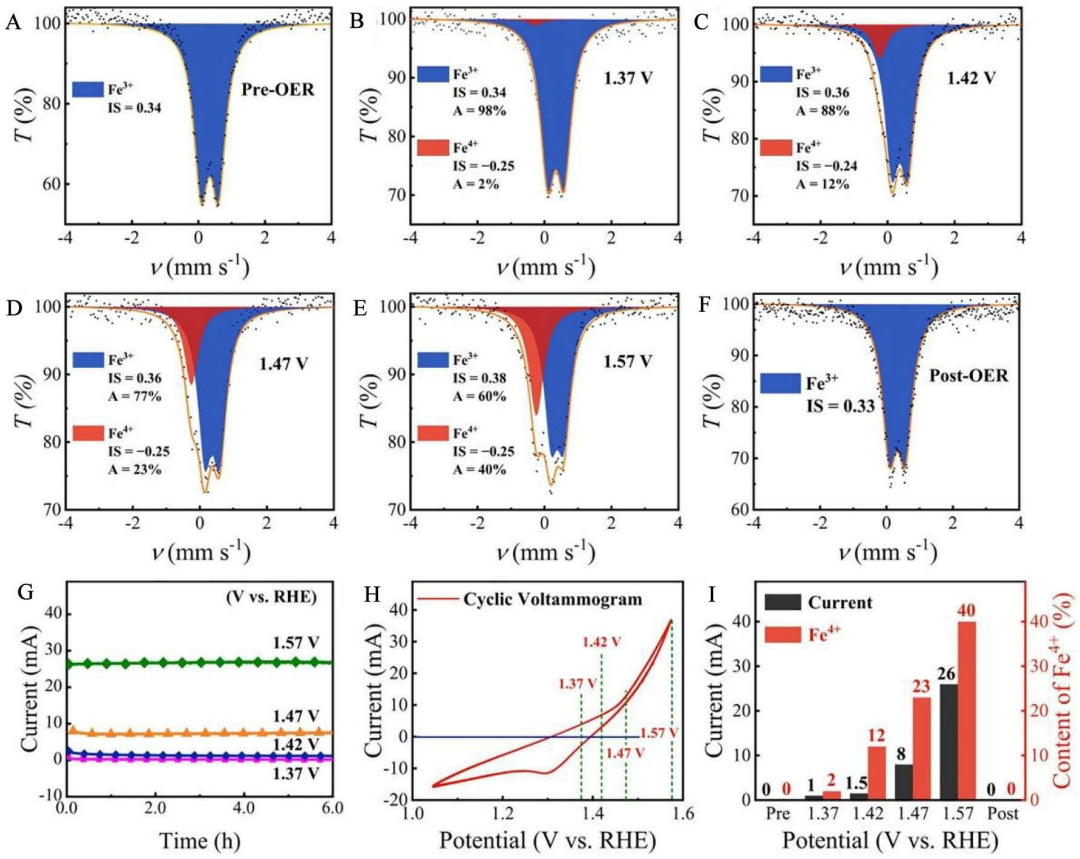

Figure 15 The *in-situ*/*operando* ^{57}Fe Mössbauer spectra of $NiFe_{0.2}$-O_xH_y collected at (A) the open circuit voltage, (B) 1.37 V, (C) 1.42 V, (D) 1.47 V, and (E) 1.57 V (vs. RHE). (F) *Ex-situ* ^{57}Fe Mössbauer spectrum of $NiFe_{0.2}$-O_xH_y collected after OER. The unit of ^{57}Fe Mössbauer parameter of isomer shift (δ) is mm·s^{-1} relative to standard α-Fe foil. (G) The current-time curves at different applied potentials obtained during the *in-situ*/*operando* measurements. (H) Cyclic voltammogram without i_R correction of $NiFe_{0.2}$-O_xH_y recorded during the *in-situ*/*operando* measurements. (I) The content of Fe^{4+} and corresponding electric current determined at different applied potentials[66]. Copyright 2021. ELSEVIER B.V. Reproduced with permission. (color on line)

Table 3 The content of high-valent iron *in-situ* produced in the $NiFe_{0.2}$-O_xH_y electrocatalyst during the oxygen evolution reaction.

This work[65] ($NiFe_{0.2}$-O_xH_y)			Previous report[47] (Layered 3:1 NiFe oxyhydroxide)		
Potential (V vs. RHE)	Fe^{4+}		Potential (V vs. RHE)	Fe^{4+}	
	Fe^{4+} (%)	δ/Fe (mm·s^{-1})		Fe^{4+} (%)	δ/Fe (mm·s^{-1})
1.32	0	-	-	-	-
1.37	2	-0.25	-	-	-
1.42 (around onset)	12	-0.24	1.49 (around onset)	0	-
1.47	23	-0.25	-	-	-
1.52	36	-0.24	-	-	-
1.57	40	-0.25	1.62	12	-0.27
-	-	-	1.76	21	-0.25

Fe^{4+} has critical role in OER as shown in the last Figure 15(I). Therefore, it can be concluded that the amount of high-valent iron species *in-situ* produced in the $NiFe_{0.2}$- (oxy)hydroxide has a positive correlation with its water oxidation reaction performance, which further deepens the understanding in the mechanism of NiFe-based electrocatalysts.

7 Summary

In this tutorial review, $NiFe_m$-Fe PBAs are used as probe precursors for preparing highly efficient NiFe-(oxy)hydroxide ($NiFe_m$-O_xH_y) OER electrocatalysts by a novel topotactic transformation method and the home-made *in-situ*/*operando* electrochemical ^{57}Fe Mössbauer spectroscopic technology independently developed is used to conduct in-depth research on the OER real active intermediates and working mechanism. Here we introduced in detail the application of *in-situ*/*operando* ^{57}Fe Mössbauer technique in the electrochemical OER test process, including its working principle, instrumentation, the design of reaction cell, NiFe-based OECs sample detection, data analysis, simulation and study case results discussion. The *in-situ*/*operando* ^{57}Fe Mössbauer technique has also been successfully applied in the ORR, CO_2RR, etc., the authors hope to be able to provide a high level of research tool for the preparation of highly efficient catalysts of electrolytic water, carbon dioxide reduction, fuel cell development and even for detecting the structural and electronic properties of single atom model catalysts.

The low cost, excellent OER activity, and better stability of NiFe-based catalysts make them ideal candidates. In order to develop novel NiFe-based OECs and their use in commercial applications, firstly, it is crucial to understand the OER process of NiFe-based OECs under realistic working conditions and to investigate their structure-activity relationship. Recently, several *in-situ*/*operando* characterization techniques have been developed to study the OER process at the solid/liquid interfaces under real-time applied potential to understand how the chemical and electronic structure changes take place in NiFe-based catalysts, the effect of electrochemical environment, and reaction intermediates interacting with each other. The focus of all these *in-situ*/*operando* techniques was to investigate the transformation of $Ni(OH)_2$ to NiOOH and the changes in oxidation states of Ni and Fe. And most of the results indicated that NiOOH is an active phase for OER, while both Ni and Fe are important for high OER activity in NiFe-based OECs. But all these *in-situ*/*operando* characterizations could not bring researchers to reach a consensus whether Fe is an active site or Ni as some *in-situ*/*operando* results indicated that Fe acts as an active site for OER, while NiOOH helps in the stabilization of Fe^{4+}[75]. On the other hand, some others suggested that Ni is the active OER center as α-$Ni(OH)_2$ nanostructure showed better OER activity compared to RuO_2[76]. Moreover, the optimal interaction strength of Ni with OH_{ad} also satisfies the Sabatier criteria for the required design of OER catalysts[29]. There could be several factors that are considered as the potential factors for different active sites during *in-situ*/*operando* characterizations. For example, during *in-situ*/*operando* studies, it becomes difficult to find out real active sites in the presences of several other disturbing factors while focusing on selective intermediates. Another factor is the different configurations of *in-situ*/*operando* cells for the study of materials under *in-situ*/*operando* conditions. As per the current status of *in-situ*/*operando* characterizations analysis, not any single technique has shown comprehensively the ability to study the phase transformation, changes in valence state and variation in morphology under OER.

Mössbauer spectroscopy is a powerful technique to study the local electronic structure, local coordination, bonding, and oxidation states of the element under an investigation in nanostructure materials. Moreover, it can help in the identification of the several *in-situ*/*operando* redox processes characterizing the intermediate phases which lead to understand the possible catalytic reaction mechanisms and pathways. Recently, Mössbauer spectroscopy has gained huge attention in electrocatalysis where it has been found more useful for the detection of primary active sites in different Fe-based materials. A deep understanding

of probing the local electronic structure, identifying the active sites and phases, determining the crystal structure, and tracking the oxidation state and environment change of various Fe-based catalysts is critical for further development in catalysis fields. For instance, the active sites of NiFe-based OECs could be clearly probed with the development of *quasi-in-situ* cells to *in-situ*/*operando* analyze the properties of catalysts. Further development of high temperature *in-situ*/*operando* or *quasi in-situ* cells would greatly promote the investigation in the phase transformation of Fe-based materials.

To address key problems, more comprehensive *in-situ*/*operando* techniques are highly desired to determine the active sites accurately and the variation in morphologies of NiFe-based catalysts under OER conditions, and those techniques influencing the interfacial interaction between catalysts and electrolyte/electrodes are crucial to be investigated simultaneously. For example, transmission and scanning electron microscopies may detect surface reconstruction and interface structure if they can overcome the difficulties of utilizing liquid electrolytes in a high vacuum environment. Although NiFe-based electrocatalysts have shown excellent OER activity, but lack of long-term stability prevents them from use in commercial applications. Therefore, understanding about degradation mechanism of catalysts, which includes variations in morphology, composition, crystal structure, and the number of active sites, is very important to design stable and highly active materials. This demands a precise and set of combining multiple complementary *in-situ*/*operando* characterization techniques to detect all the above-mentioned changes simultaneously. Hence, it will be beneficial to understand the activity-structure relationship in different catalysts by combining different *in-situ*/*operando* characterization techniques and theoretical calculations to determine the active sites for OER. This will help in understanding the OER mechanisms comprehensively, and will guide the design of the robust and efficient catalysts for OER to commercial applications.

Acknowledgements

This work was financially supported by the National Natural Science Foundation of China (No.: 21961142006) and the International Partnership Program of Chinese Academy of Sciences (No.: 121421KYSB20170020).

References:

[1] Chu S, Majumdar A. Opportunities and challenges for a sustainable energy future[J]. Nature, 2012, 488(7411): 294-303.

[2] Fu J, Cano Z P, Park M G, Yu A, Fowler M, Chen Z W. Electrically rechargeable zinc-air batteries: progress, challenges, and perspectives[J]. Adv. Mater., 2017, 29(7): 1604685.

[3] Zhang H W, Shen P K. Recent development of polymer electrolyte membranes for fuel cells[J]. Chem. Rev., 2012, 112(5): 2780-2832.

[4] Jiao K, Xuan J, Du Q, Bao Z M, Xie B A, Wang B W, Zhao Y, Fan L H, Wang H Z, Hou Z L, Huo S, Brandon N P, Yin Y, Guiver M D. Designing the next generation of proton-exchange membrane fuel cells[J]. Nature, 2021, 595 (7867): 361-369.

[5] Johnson D, Qiao Z, Djire A. Progress and challenges of carbon dioxide reduction reaction on transition metal based electrocatalysts[J]. ACS Appl. Energy Mater., 2021, 4(9): 8661-8684.

[6] Li Y J, Sun Y J, Qin Y N, Zhang W Y, Wang L, Luo M C, Yang H, Guo S J. Recent advances on water-splitting electrocatalysis mediated by noble-metal-based nanostructured materials[J]. Adv. Energy Mater., 2020, 10(11): 1903120.

[7] Li J C, Kuang Y, Meng Y T, Tian X, Hung W H, Zhang X, Li A W, Xu M Q, Zhou W, Ku C S, Chiang C Y, Zhu G Z, Guo J Y, Sun X M, Dai H J. Electroreduction of CO_2 to formate on a copper-based electrocatalyst at high pressures with high energy conversion efficiency[J]. J. Am. Chem. Soc., 2020, 142(16): 7276-7282.

[8] Wang M Y, Wang Z, Gong X Z, Guo Z C. The intensification technologies to water electrolysis for hydrogen production-A review[J]. Renew. Sust. Energ. Rev., 2014, 29: 573-588.

[9] Mei L, Gao X P, Gao Z, Zhang Q Y, Yu X G, Rogach A L, Zeng Z Y. Size-selective synthesis of platinum nanoparticles on transition-metal dichalcogenides for the hydrogen evolution reaction[J]. Chem. Commun., 2021, 57 (23): 2879-2882.

[10] Yu J, He Q J, Yang G M, Zhou W, Shao Z P, Ni M. Re

cent advances and prospective in ruthenium-based materials for electrochemical water splitting[J]. ACS Catal., 2019, 9(11): 9973-10011.

[11] Hu C L, Zhang L, Gong J L. Recent progress made in the mechanism comprehension and design of electrocatalysts for alkaline water splitting[J]. Energy Environ. Sci., 2019, 12(9): 2620-2645.

[12] Lyons M E G, Floquet S. Mechanism of oxygen reactions at porous oxide electrodes. Part 2-Oxygen evolution at RuO_2, IrO_2 and $Ir_xRu_{1-x}O_2$ electrodes in aqueous acid and alkaline solution[J]. Phys. Chem. Chem. Phys., 2011, 13 (12): 5314-5335.

[13] Hunter B M, Gray H B, Muller A M. Earth-abundant heterogeneous water oxidation catalysts[J]. Chem. Rev., 2016, 116(22): 14120-14136.

[14] Suen N T, Hung S F, Quan Q, Zhang N, Xu Y J, Chen H M. Electrocatalysis for the oxygen evolution reaction: recent development and future perspectives[J]. Chem. Soc. Rev., 2017, 46(2): 337-365.

[15] Lee Y, Suntivich J, May K J, Perry E E, Shao-Horn Y. Synthesis and activities of rutile IrO_2 and RuO_2 nanoparticles for oxygen evolution in acid and alkaline solutions [J]. J. Phys. Chem. Lett., 2012, 3(3): 399-404.

[16] Blakemore J D, Schley N D, Kushner-Lenhoff M N, Winter A M, D'Souza F, Crabtree R H, Brudvig G W. Comparison of amorphous iridium water-oxidation electrocatalysts prepared from soluble precursors[J]. Inorg. Chem., 2012, 51(14): 7749-7763.

[17] Dionigi F, Zhu J, Zeng Z H, Merzdorf T, Sarodnik H, Gliech M, Pan L J, Li W X, Greeley J, Strasser P. Intrinsic electrocatalytic activity for oxygen evolution of crystalline 3d-transition metal layered double hydroxides[J]. Angew. Chem. Int. Edit., 2021, 60(26): 14446-14457.

[18] Han L, Dong S L, Wang E K. Transition-metal (Co, Ni, and Fe)-based electrocatalysts for the water oxidation reaction[J]. Adv. Mater., 2016, 28(42): 9266-9291.

[19] Zhang Q Y, Mei L, Cao X H, Tang Y X, Zeng Z Y. Intercalation and exfoliation chemistries of transition metal dichalcogenides[J]. J. Mater. Chem. A, 2020, 8(31): 15417-15444.

[20] Han N, Liu P Y, Jiang J, Ai L H, Shao Z P, Liu S M. Recent advances in nanostructured metal nitrides for water splitting[J]. J. Mater. Chem. A , 2018, 6(41): 19912-19933.

[21] Zhang H J, Maijenburg A W, Li X P, Schweizer S L, Wehrspohn R B. Bifunctional heterostructured transition metal phosphides for efficient electrochemical water splitting[J]. Adv. Funct. Mater., 2020, 30(34): 2003261.

[22] Gupta S, Patel M K, Miotello A, Patel N. Metal boride-based catalysts for electrochemical water-splitting: A review[J]. Adv. Funct. Mater., 2020, 30(1): 1906481.

[23] Wang H P, Zhu S, Deng J W, Zhang W C, Feng Y Z, Ma J M. Transition metal carbides in electrocatalytic oxygen evolution reaction[J]. Chin. Chem. Lett., 2021, 32(1): 291-298.

[24] Zhang B, Zheng Y J, Ma T, Yang C D, Peng Y F, Zhou Z H, Zhou M, Li S, Wang Y H, Cheng C. Designing MOF nanoarchitectures for electrochemical water splitting[J]. Adv. Mater., 2021, 33(17): 2006042.

[25] Balogun M S, Huang Y C, Qiu W T, Yang H, Ji H B, Tong Y X. Updates on the development of nanostructured transition metal nitrides for electrochemical energy storage and water splitting[J]. Mater. Today, 2017, 20(8): 425-451.

[26] Jin S. Are metal chalcogenides, nitrides, and phosphides oxygen evolution catalysts or bifunctional catalysts? [J] ACS Energy Lett., 2017, 2(8): 1937-1938.

[27] Dionigi F, Strasser, P. NiFe-based (oxy)hydroxide catalysts for oxygen evolution reaction in non-acidic electrolytes[J]. Adv. Energy Mater., 2016, 6 (23): 1600621.

[28] Gong M, Li Y G, Wang H L, Liang Y Y, Wu J Z, Zhou J G, Wang J, Regier T, Wei F, Dai H J. An advanced Ni-Fe layered double hydroxide electrocatalyst for water oxidation[J]. J. Am. Chem. Soc., 2013, 135(23): 8452-8455.

[29] Subbaraman R, Tripkovic D, Chang K C, Strmcnik D, Paulikas A P, Hirunsit P, Chan M, Greeley J, Stamenkovic V, Markovic N M. Trends in activity for the water electrolyser reactions on 3d M (Ni, Co, Fe, Mn) hydr(oxy) oxide catalysts[J]. Nat. Mater., 2012, 11(6): 550-557.

[30] Munshi M Z A, Tseung A C C, Parker J. The dissolution of iron from the negative material in pocket plate nickel-cadmium batteries[J]. J. Appl. Electrochem., 1985, 15 (5): 711-717.

[31] Tichenor R L. Nickel oxides-relation between electrochemical and foreign ion content[J]. J. Ind. Eng. Chem., 1952, 44(5), 973-977.

[32] Corrigan D A. The catalysis of the oxygen evolution reaction by iron impurities in thin film nickel oxide electrodes[J]. J. Electrochem. Soc., 1987, 134(2): 377-384.

[33] Zhu K Y, Liu H Y, Li M R, Li X N, Wang J H, Zhu X F, Yang W S. Atomic-scale topochemical preparation of crystalline Fe^{3+}-doped β-$Ni(OH)_2$ for an ultrahigh-rate oxygen evolution reaction[J]. J. Mater. Chem. A, 2017, 5 (17): 7753-7758.

[34] Stevens M B, Trang C D M, Enman L J, Deng J, Boettcher S W. Reactive Fe-sites in Ni/Fe(oxy)hydroxide are responsible for exceptional oxygen electrocatalysis activity[J].

J. Am. Chem. Soc., 2017, 139(33): 11361-11364.

[35] Młynarek G, Paszkiewicz M, Radniecka A. The effect of ferric ions on the behaviour of a nickelous hydroxide electrode[J]. J. Appl. Electrochem., 1984, 14(2): 145-149.

[36] Trotochaud L, Young S L, Ranney J K, Boettcher S W. Nickel-iron oxyhydroxide oxygen-evolution electrocatalysts: the role of intentional and incidental iron incorporation[J]. J. Am. Chem. Soc., 2014, 136(18): 6744-6753.

[37] Görlin M, Chernev P, de Araújo J F, Reier T, Dresp S, Paul B, Krähnert R, Dau H, Strasser P. Oxygen evolution reaction dynamics, faradaic charge efficiency, and the active metal redox states of Ni-Fe oxide water splitting electrocatalysts[J]. J. Am. Chem. Soc., 2016, 138(17): 5603-5614.

[38] Görlin M, de Araújo J F, Schmies H, Bernsmeier D, Dresp S, Gliech M, Jusys Z, Chernev P, Kraehnert R, Dau H, Strasser P. Tracking catalyst redox states and reaction dynamics in Ni-Fe oxyhydroxide oxygen evolution reaction electrocatalysts: the role of catalyst support and electrolyte pH[J]. J. Am. Chem. Soc., 2017, 139(5): 2070-2082.

[39] Hunter B M, Thompson N B, Müller A M, Rossman G R, Hill M G, Winkler J R, Gray H B. Trapping an iron(VI) water-splitting intermediate in nonaqueous media[J]. Joule, 2018, 2(4): 747-763.

[40] Ahn H S, Bard A J. Surface interrogation scanning electrochemical microscopy of $Ni_{1-x}Fe_xOOH$ ($0 < x < 0.27$) oxygen evolving catalyst: Kinetics of the "fast" iron sites[J]. J. Am. Chem. Soc., 2016, 138(1): 313-318.

[41] Klaus S, Cai Y, Louie M W, Trotochaud L, Bell A T. Effects of Fe electrolyte impurities on $Ni(OH)_2$/NiOOH structure and oxygen evolution activity[J]. J. Phys. Chem. C, 2015, 119(13): 7243-7254.

[42] Zou S H, Burke M S, Kast M G, Fan J, Danilovic N, Boettcher S W. Fe (oxy) hydroxide oxygen evolution reaction electrocatalysis: intrinsic activity and the roles of electrical conductivity, substrate, and dissolution[J]. Chem. Mater., 2015, 27(23): 8011-8020.

[43] Friebel D, Louie M W, Bajdich M, Sanwald K E, Cai Y, Wise A M, Cheng M J, Sokaras D, Weng T C, Alonso-Mori R, Davis R C, Bargar J R, Norskov J K, Nilsson A, Bell A T. Identification of highly active Fe sites in (Ni, Fe) OOH for electrocatalytic water splitting[J]. J. Am. Chem. Soc., 2015, 137(3): 1305-1313.

[44] Chen S C, Kang Z X, Zhang X D, Xie J F, Wang H, Shao W, Zheng X S, Yan W S, Pan B C, Xie Y. Highly active Fe sites in ultrathin pyrrhotite Fe_7S_8 nanosheets realizing efficient electrocatalytic oxygen evolution[J]. ACS Central Sci., 2017, 3(11): 1221-1227.

[45] Xiao H, Shin H, Goddard W A. Synergy between Fe and Ni in the optimal performance of (Ni,Fe)OOH catalysts for the oxygen evolution reaction[J]. Proc. Natl. Acad. Sci. U.S.A., 2018, 115(23): 5872-5877.

[46] Corrigan D A, Conell R S, Fierro C A, Scherson D A. *In-situ* Moessbauer study of redox processes in a composite hydroxide of iron and nickel[J]. J. Phys. Chem., 1987, 91(19): 5009-5011.

[47] Chen J Y C, Dang L N, Liang H F, Bi W L, Gerken J B, Jin S, Alp E E, Stahl S S. Operando analysis of NiFe and Fe oxyhydroxide electrocatalysts for water oxidation: Detection of Fe^{4+} by Mössbauer spectroscopy[J]. J. Am. Chem. Soc., 2015, 137(48): 15090-15093.

[48] Tao H B, Xu Y H, Huang X, Chen J Z, Pei L J, Zhang J M, Chen J G G, Liu B. A general method to probe oxygen evolution intermediates at operating conditions[J]. Joule, 2019, 3(6): 1498-1509.

[49] Su X Z, Wang Y, Zhou J, Gu S Q, Li J, Zhang S. *Operando* spectroscopic identification of active sites in NiFe prussian blue analogues as electrocatalysts: Activation of oxygen atoms for oxygen evolution reaction[J]. J. Am. Chem. Soc., 2018, 140(36): 11286-11292.

[50] Shinagawa T, Garcia-Esparza A T, Takanabe K. Insight on Tafel slopes from a microkinetic analysis of aqueous electrocatalysis for energy conversion[J]. Sci. Rep., 2015, 5: 13801.

[51] Deng Y L, Yeo B S. Characterization of electrocatalytic water splitting and CO_2 reduction reactions using *in situ*/*operando* Raman spectroscopy[J]. ACS Catal., 2017, 7(11): 7873-7889.

[52] Timoshenko J, Cuenya B R. *In situ*/*operando* electrocatalyst characterization by X-ray absorption spectroscopy[J]. Chem. Rev., 2020, 121(2): 882-961.

[53] Li X N, Wang H Y, Yang H B, Cai W Z, Liu S, Liu B. *In situ*/*operando* characterization techniques to probe the electrochemical reactions for energy conversion[J]. Small Methods, 2018, 2(6): 1700395.

[54] Zeng Y Q, Li X N, Wang J H, Sougrati M T, Huang Y Q, Zhang T, Liu B. *In situ*/*operando* Mössbauer spectroscopy for probing heterogeneous catalysis[J]. Chem. Catal., 2021, 1(6): 1215-1233.

[55] Qiu Z, Tai C W, Niklasson G A, Edvinsson T. Direct observation of active catalyst surface phases and the effect of dynamic self-optimization in NiFe-layered double hydroxides for alkaline water splitting[J]. Energy Environ. Sci., 2019, 12(2): 572-581.

[56] Stoerzinger K A, Hong W T, Crumlin E J, Bluhm H, Shao-Horn Y. Insights into electrochemical reactions from ambient pressure photoelectron spectroscopy[J]. Accounts

Chem. Res., 2015, 48(11): 2976-2983.

[57] Ali-Löytty H, Louie M W, Singh M R, Li L, Casalongue H G S, Ogasawara H, Crumlin E J, Liu Z, Bell A T, Nilsson A, Friebel D. Ambient-pressure XPS study of a Ni-Fe electrocatalyst for the oxygen evolution reaction[J]. J. Phys. Chem. C, 2016, 120(4): 2247-2253.

[58] Li X N, Zhu K Y, Pang J F, Tian M, Liu J Y, Rykov A I, Zheng M Y, Wang X D, Zhu X F, Huang Y Q, Liu B, Wang J H, Yang W S, Zhang T. Unique role of Mössbauer spectroscopy in assessing structural features of heterogeneous catalysts[J]. Appl. Catal. B-Environ., 2018, 224: 518-532.

[59] Mössbauer R L. Kernresonanzfluoreszenz von gammastrahlung in Ir191[J]. Zeitschrift für Physik, 1958, 151(2): 124-143.

[60] Liu K, Rykov A I, Wang J H, Zhang T. Recent advances in the application of Mössbauer spectroscopy in heterogeneous catalysis[J]. Adv. Catal., 2015, 58: 1-142.

[61] Kramm U I, Ni L M, Wagner S. ^{57}Fe Mössbauer spectroscopy characterization of electrocatalysts[J]. Adv. Mater., 2019, 31(31): 1805623.

[62] Fischer N, Claeys M. *In situ* characterization of Fischer-Tropsch catalysts: A review[J]. J. Phys. D-Appl. Phys., 2020, 53(29): 293001.

[63] Gütlich P, Bill E, Trautwein A X. Mössbauer spectroscopy and transition metal chemistry: Fundamentals and applications[M]. Deutschland: Springer, 2010.

[64] Wang J H, Jin C Z, Liu X, Liu D R, Sun H, Wei F F, Zhang T, Stevens J G, Khasanov A, Khasanova I. Mössbauer spectroscopy database: Past, present, future[J]. Hyperfine Interact., 2012, 204(1-3): 111-117.

[65] Klencsár Z. MossWinn-methodological advances in the field of Mössbauer data analysis[J]. Hyperfine Interact., 2013, 217(1-3): 117-126.

[66] Kuang Z C, Liu S, Li X N, Wang M, Ren X Y, Ding J, Ge R L, Zhou W H, Rykov A I, Sougrati M T, Lippens P E, Huang Y Q, Wang J H. Topotactically constructed nickel-iron (oxy)hydroxide with abundant *in-situ* produced high-valent iron species for efficient water oxidation[J]. J. Energy Chem., 2021, 57: 212-218.

[67] Li X N, Ao Z M, Liu J Y, Sun H Q, Rykov A I, Wang J H. Topotactic transformation of metal-organic frameworks to graphene-encapsulated transition-metal nitrides as efficient Fenton-like catalysts[J]. ACS Nano, 2016, 10 (12): 11532-11540.

[68] Catala L, Mallah T. Nanoparticles of Prussian blue analogs and related coordination polymers: From information storage to biomedical applications[J]. Coord. Chem. Rev., 2017, 346: 32-61.

[69] Zakaria M B, Chikyow T. Recent advances in Prussian blue and Prussian blue analogues: Synthesis and thermal treatments[J]. Coord. Chem. Rev., 2017, 352: 328-345.

[70] Hu M, Belik A A, Imura M, Mibu K, Tsujimoto Y, Yamauchi Y. Synthesis of superparamagnetic nanoporous iron oxide particles with hollow interiors by using prussian blue coordination polymers[J]. Chem. Mater., 2012, 24(14): 2698-2707.

[71] Li X N, Wang Z H, Zhang B, Rykov A I, Ahmed M A, Wang J H. $Fe_xCo_{3-x}O_4$ nanocages derived from nanoscale metal-organic frameworks for removal of bisphenol A by activation of peroxymonosulfate[J]. Appl. Catal. B-Environ., 2016, 181: 788-799.

[72] Li X N, Cao C S, Hung S F, Lu Y R, Cai W Z, Rykov A I, Miao S, Xi S B, Yang H B, Hu Z H, Wang J H, Zhao J Y, Alp E E, Xu W, Chan T S, Chen H M, Xiong Q H, Xiao H, Huang Y Q, Li J, Zhang T, Liu B. Identification of the electronic and structural dynamics of catalytic centers in single-Fe-atom material[J]. Chem, 2020, 6(12): 3440-3454.

[73] Li X N, Zeng Y Q, Tung C W, Lu Y R, Baskaran S, Hung S F, Wang S F, Xu C Q, Wang J H, Chan T S, Chen H M, Jiang J C, Yu Q, Huang Y Q, Li J, Zhang T, Liu B. Unveiling the *in situ* generation of a monovalent Fe(I) site in the single-Fe-atom catalyst for electrochemical CO_2 reduction[J]. ACS Catal., 2021, 11(12): 7292-7301.

[74] Li J K, Sougrati M T, Zitolo A, Ablett J M, Oğuz I C, Mineva T, Matanovic I, Atanassov P, Huang Y, Zenyuk I, Di Cicco A, Kumar K, Dubau L, Maillard F, Dražic G, Jaouen F. Identification of durable and non-durable FeN_x sites in Fe-N-C materials for proton exchange membrane fuel cells[J]. Nature. Catal., 2020, 4(1): 10-19.

[75] Zhu K Y, Zhu X F, Yang W S. Application of *in-situ* techniques for the characterization of NiFe-based oxygen evolution reaction (OER) electrocatalysts[J]. Angew. Chem. Int. Ed., 2019, 58(5): 1252-1265.

[76] Gao M R, Sheng W C, Zhuang Z B, Fang Q R, Gu S, Jiang J, Yan Y S. Efficient water oxidation using nanostructured α-nickel-hydroxide as an electrocatalyst[J]. J. Am. Chem. Soc., 2014, 136(19): 7077-7084.

原位 ^{57}Fe 穆斯堡尔光谱技术及其在 Ni-Fe 基析氧反应电催化剂中的应用

Jafar Hussain Shah[1], 谢起贤[2], 匡智崇[1], 格日乐[1], 周雯慧[1], 刘朵绒[1], Alexandre I. Rykov[1], 李旭宁[1], 罗景山[2], 王军虎[1*]

(1. 中国科学院大连化学物理研究所, 大连 116023; 2. 南开大学, 天津 300350)

摘要: 近年来, 析氧反应(oxygen evolution reaction)中针对高效且具有成本效益的电催化剂开发一直是构筑有效利用可再生能源存储系统和水分解生产清洁氢能燃料的重大障碍。OER 过程涉及四电子、四质子耦合并形成氧-氧(O-O)键, 因此动力学上进程缓慢。为提升其在水分解产氢及二氧化碳还原反应中的应用, 需要开发高效催化剂, 降低 OER 过电位, 以减轻能量转换过程中固有的能量损失。研究表明, IrO_2 和 RuO_2 具有较低析氧过电位, 但储量低、价格昂贵, 大大限制了其在析氧反应中的大规模应用。而 Ni-Fe 基析氧催化剂在碱性水分解反应中展现了优异的性能, 其在水分解过程中的催化机制仍有待进一步研究。

为了解决 Ni-Fe 基催化剂在析氧反应过程中反应位点及催化反应机制等关键问题, 迫切需要更先进的原位技术来准确表征, 原位追踪催化剂形态变化与电解质/电极之间的界面相互作用的影响。光谱与电化学结合的原位技术可以监测析氧反应过程催化剂自身的变化。目前, 已有大量原位光谱技术与电化学进行结合, 揭示 Ni-Fe 基催化剂在 OER过程中的反应机理及活性位点, 包括原位表面增强拉曼光谱、原位同步辐射 X 射线吸收光谱、原位紫外-可见光谱、原位扫描电化学显微镜及原位穆斯堡尔光谱等。其中, 原位拉曼技术可以观察 Ni-Fe 催化剂的振动, 可以在电解液中施加测试电压条件下监测电化学反应过程中的中间体, 从而提供实时反应信息, 有助于追踪电化学驱动反应是如何发生的。原位同步辐射技术可以研究OER 过程中 Ni-Fe 催化剂材料的电子结构和局部几何结构的信息, 但目前的研究中更多的是探究 Ni 的价态变化, 对 Fe 的研究信息较少。原位紫外-可见光谱也主要是针对 $Ni(OH)_2$ 的变化展开研究, 逐渐提高施加电位, $Ni(OH)_2$ 会向着 NiOOH 逐渐变化, 紫外-可见技术可以追踪 Ni-Fe 基电催化剂中的金属氧化过程。众多电化学原位光谱技术中, ^{57}Fe 穆斯堡尔谱因具有超高的能量分辨率, 是确定催化剂相结构、鉴定活性位点、阐明催化机理以及确定催化活性与催化剂配位结构之间关系的最佳手段。此外, 原位穆斯堡尔光谱技术基于原子核和核外电子的超精细相互作用而给出的同质异能移、四极矩分裂以及有效磁场等针对催化剂中的 Fe 位点的氧化态、电子自旋构型、对称性和磁性信息进行研究, 为 Ni-Fe 基催化剂在析氧反应中的应用提供强有力的支持。

1957 年, 德国科学家鲁道夫·路德维希·穆斯堡尔(Rudolf Ludwig Mössbauer)在其 27 岁时, 发现作为晶格谐振子的原子在发射或吸收 γ 射线时以一定的概率不会改变它们的量子力学状态, 而这一 γ 射线的核共振吸收现象于 1961 年获得诺贝尔物理学奖, 不久后被命名为穆斯堡尔效应。穆斯堡尔效应是来自于无反冲的 γ 射线吸收和发射的核共振现象, 能量 E_e 处于激发态的原子核(Z 质子和 N 中子)通过产生能量为 E_γ 的 γ 射线跃迁到能量为 E_g 的基态, γ 射线可能会被处于基态的另一个相同类型的原子核(相同的 Z 和 N)吸收, 从而转变为能量 E_e 的激发态。只有当发射线和吸收线足够重叠时, 才能看到共振吸收。

原位穆斯堡尔谱在 Ni-Fe 催化剂析氧反应中应用, 首先需要搭建 ^{57}Fe 穆斯堡尔谱仪与电化学工作站联用。标准的穆斯堡尔光谱仪主要由放射源(通常是 ^{57}Co 在 Rh 或 Pd 金属基质中用于 ^{57}Fe 穆斯堡尔光谱)、速度传感器、速度校准装置、波形发生器和同步器、γ 射线检测系统、多通道分析仪、计算机, 并且可选配低温恒温器或高温烘箱, 以控制测量过程处于适宜温度。实际测试过程中, 穆斯堡尔谱可以通过速度扫描方法生成, 利用移动驱动器或速度传感器以特定速度重复移动源或样品(所谓的多普勒运动), 同时 γ 射线连续传输或发射穿过样品并计数在同步通道上。获得穆斯堡尔谱图后, 基于穆斯堡尔谱数据库(https://medc.dicp.ac.cn/, 由中国科学院大连化学研究所穆斯堡尔效应数据中心从全世界收集的穆斯堡尔谱样品数据), 对 ^{57}Fe 穆斯堡尔谱进行分析拟合, 对含 Fe 基材料的物相、价态、自旋态和配位结构进行归因和分析。数据分析拟合主要利用 MossWinn 数据分析和拟合软件(http://www.mosswinn.com/)。以 Ni-Fe 氢氧化物催化剂为例, 对于原始催化剂, 其仅存在一种 Fe^{3+} 物种, 当该催化剂参与 OER 过程后, 可能会存在 Fe^{4+}, 在双峰基础上, 拟合结果中则会出现肩峰向负侧移动现象, 可以确认高价

Fe 的存在,例如 Fe^{4+}。为充分证明高价 Fe 的存在,对于 Ni-Fe 基催化剂的穆斯堡尔谱测试,还需在工况条件下进行原位测试。

20 世纪 80 年代后期,非贵金属氧化物和氢氧化物代替贵金属氧化物阳极催化剂的电解水研究开始受到关注。Corrigan 等通过将 Fe 杂质引入 NiO 阳极,测试过程中发现 OER 活性会增加,但后续的研究中对于 Fe 究竟如何改变 Ni基催化剂的 OER 性能仍旧不清晰。尔后,原位穆斯堡尔谱的引入逐渐揭开 Fe 在 Ni-Fe 电催化水分解析氧反应中的作用。为提高测试准确性并保证穆斯堡尔谱信号的稳定,本实验室对原位穆斯堡尔谱装置做了开发和改进。主要包括三部分:(1) 穆斯堡尔光谱仪,(2) 电化学工作站,以及(3) 自主设计的原位 OER 电化学反应池。在我们的实验室中,使用了具有 14.4 keV 级 γ 射线的单线^{57}Fe 穆斯堡尔谱放射源 ^{57}Co(Rh),可以减少电解液中的信号衰减并获得令人满意的信噪比,附带 CHI660E 电化学工作站。对于常规的 OER 测试,在室温 298 K 条件下进行测试,测试前首先用 α-Fe 对穆斯堡尔谱仪进行多普勒速度校准,在进行原位穆斯堡尔谱-OER 实验之前,电解液用氮气或氩气饱和以去除溶解的氧气。为了保证测试信号的准确性,实验中所使用的电解池不含任何 Fe 杂质,因此采用了 Teflon 材料。为避免测试过程中产生的 O_2 气泡对信号产生干扰,可以采用蠕动泵循环电解液,并且保证测试过程中局部的微反应环境的一致性。对于普通 OER 测试,仅需要少量催化剂,但对于原位 ^{57}Fe 穆斯堡尔谱测试,只有保证 Ni-Fe 催化剂中 ^{57}Fe 含量充足的条件下,才可以获得高质量信号。但 OER 过程中,不建议催化剂载量过高,催化过程中主要是表面催化剂在反应,当样品过厚时,深层样品无法参与析氧反应过程,可能会有部分 Fe 仍旧维持 Fe^{3+} 状态。通常,对于常规 ^{57}Fe 穆斯堡尔光谱测量的催化剂,若在制备中使用普通 Fe 源,则需要 Fe 含量在 5 ~ 10 mg·cm^{-2},这其中仅有 ~2.2%的自然丰度 ^{57}Fe同位素,需要长时间监测才可以采集到信号。为保证实验的顺利进行,可以在样品制备过程中直接使用 ^{57}Fe 源,方便快捷采集高质量信号。为了保证样品测试的准确性,在 OER开始前,我们可以在同一电解液中,在开路电位(OCP)下,对其进行测试,这一原始样品的测试可与后续施加电位的 Ni-Fe 催化剂测试结果进行对比。有外加电压测试时,需要保证催化剂处于稳定状态下进行测试,整个测试过程中保持电流密度稳定,这不仅可以保证催化剂的稳定性,还有助于确定催化剂的真实结构。

利用原位 ^{57}Fe 穆斯堡尔谱,我们对通过 Ni-Fe 普鲁士蓝类似物原位拓扑转换获得的 Ni-Fe 羟基氧化物电催化剂进行了测试。基于原位拉曼技术,我们发现在阳极电位下,Ni-Fe 催化剂中 α-Ni(OH)$_2$ 相会不可逆转变为 γ-NiOOH。原位 ^{57}Fe 穆斯堡尔谱测试结果表明,在较低的施加电位(例如 1.22 V 和 1.32 V vs. RHE)下,Fe 在 $NiFe_{0.2}$-O_xH_y 中仅处于 +3 氧化态,其光谱结果与开路电位下 $NiFe_{0.2}$-O_xH_y 谱图相似,其中只有一个双峰,两个峰的强度相等,可归因于高自旋 Fe^{3+} 物种。但随着外加电位增加并达到 1.37 V,两个峰的强度开始变得不相等,开始出现一个小的肩峰,其同质异能移(δ)值约为 -0.25 mm·s^{-1},可以归属为 Fe^{4+} 。随着电压的逐渐增加,催化剂中的 Fe^{4+} 含量逐渐增加。在OER 过程中,施加电位 1.42 V vs. RHE 时,Fe^{4+} 含量 ~ 12%。当施加的电势达到 1.57 V 时,催化剂中 Fe^{4+} 的含量进一步增加到约 40%。这一实例充分展现了原位 ^{57}Fe 穆斯堡尔谱与 Ni-Fe 催化 OER 过程的应用,也体现了 $NiFe_{0.2}$-O_xH_y 催化剂原位产生的 Fe^{4+} 物种的量与其水氧化反应性能呈正相关,进一步加深了对 Ni-Fe 水氧化催化机理的理解。

Ni-Fe 基催化剂因其价格低廉,电催化析氧性能优异,因此成为碱性水分解析氧过程的理想候选者。虽然 Ni-Fe 基电催化剂表现出优异的 OER 活性,但缺乏长期稳定性阻碍了其在商业中的应用。因此,充分了解 Ni-Fe 催化剂的衰减机理,包括形态、组成、晶体结构和活性位点数量的变化,对于设计稳定和高效 Ni-Fe 催化材料非常重要,充分了解 Ni-Fe 催化剂在 OER 过程中的电子结构及其与析氧反应中间体的相互作用尤为重要。原位拉曼及原位紫外-可见光谱可以对 Ni-Fe 催化剂中的 Ni(OH)$_2$ 到 NiOOH 的变化进行深入探究,而原位 ^{57}Fe 穆斯堡尔谱测试则可以揭示 Ni-Fe 基催化剂中 Fe 的电子环境及其电子的、结构的和磁性的变化。穆斯堡尔光谱为研究 Ni-Fe 催化剂中 Fe 的局部电子结构、局部配位、键合和氧化态的提供了强大技术支撑。最近,穆斯堡尔光谱在电催化领域获得了越来越多的关注,它对于检测不同铁基催化材料中的主要活性位点有着重要作用。

关键词: 析氧反应;Ni-Fe 羟基氧化物电催化剂;原位电化学穆斯堡尔光谱技术;Ni-Fe 普鲁士蓝类似物;关键中间物表征